NASA Technical Memorandum 89116

FATIGUE DAMAGE ACCUMULATION IN VARIOUS METAL MATRIX COMPOSITES

W. S. Johnson

March 1987

NASA
National Aeronautics and
Space Administration

Langley Research Center
Hampton, Virginia 23665

FATIGUE DAMAGE ACCUMULATION IN VARIOUS METAL MATRIX COMPOSITES

W. S. Johnson
Senior Research Scientist
Materials Division
NASA Langley Research Center
Hampton, Virginia 23665-5225

1.0 INTRODUCTION

Historically metal matrix composites (MMC) were among the first continuous fiber-reinforced composites studied. Systems such as steel wire reinforced copper were early model systems. Over the past twenty years or so, the interest in metal matrix composites has fluctuated between mild interest and no interest. Hence, the only production continuous fiber-reinforced metal matrix composite components currently in service are the tubular struts on the United States space shuttle. The main disadvantage of continuous fiber-reinforced metal matrix composites is the high cost of the fibers and of fabrication. Cutting and drilling of some of the current systems can be very expensive compared to tradition metal shop operations. Compared to resin matrix composites, MMC may offer many attractive properties such as better environmental tolerance to moisture and temperature, higher interlaminar strength, and better impact and lightning damage resistance. Compared to normal homogeneous structural metals, MMC offer much higher stiffness to weight and strength to weight ratios. However, in both cases the advantages of MMC could not justify the additional costs.

In the mid 1980's several areas of technological advancement sparked a renewed interest in continuous fiber metal matrix composites, namely, the need for high temperature materials for aerospace structures, advanced engines, and the need for materials with a high degree of thermal dimensional stability for space antenna application. MMC have unique properties that make these technology advancements conceivable. MMC will still be very expensive, but the applications are such that polymer matrix composites and homogeneous metals will not, based on the present state-of-the-art technology, be able to meet the new requirements. Since there are many new MMC systems under consideration and development to meet projected needs, the future for MMC looks promising.

The purpose of the paper is to review some of the latest understanding of the fatigue behavior of continuous fiber reinforced metal matrix composites. The emphasis is on the development of an understanding of different fatigue damage mechanisms and why and how they occur. This paper is not intended to be a comprehensive literature review of the fatigue of metal matrix composites. The author recognizes that particulate and whisker reinforced metal matrix composites are also of current interest and have good applications potential. However, outside of a few problems associated with their orthotropic properties, these discontinuous reinforced composites have fatigue behavior which is essentially the same as homogeneous metals and will not be addressed in this paper.

Metal matrix composites consist of high strength - high stiffness fibers embedded in a metal matrix. In typical polymer matrix composites, the strengths and moduli of the fibers are always

much higher then those of the polymer matrix material, perhaps two orders of magnitude higher. In contrast, the metal matrix may have a strength and stiffness of the same order of magnitude as the fiber. The relative strength (fatigue strength in particular) of the fiber to the matrix may play a big role in determining where fatigue damage initiates and how it grows. Based on the relative strain to fatigue failure of the fiber and matrix, the possible failure modes of MMC can be grouped into three categories. Each category is illustrated below with a particular MMC system.

In boron/aluminum composites, the boron fibers are very fatigue insensitive. They are rather large diameter (0.14 mm) fibers, with very smooth sides, and are virtually elastic until fracture. Boron has a strain to failure of about 0.0085. While the strain to failure of 6061-0 aluminum is almost 0.1, it yields at a strain between 0.001 and 0.002. Therefore, under static loading the fibers would reach their critical strain first and fail before the matrix. But under fatigue loading, the matrix would cyclically yield at strain levels far below critical strains for the fibers. This cyclic yielding could result in fatigue damage to the matrix but not to the fibers. Therefore in this material, fatigue damage is matrix dominated.

In alumina fiber/aluminum composites, the alumina fibers (denoted as FP by DuPont) are very small in diameter (20×10^{-6}m) compared to the boron fibers and have a lower static strain to failure (approximately 0.003). The surface of an alumina fiber is "cobblestone" like, which may imply a low fatigue strength due to stress concentrations. In this composite system, the fibers may very well fail due to fatigue before the matrix does, thus, fatigue damage

would be fiber dominated.

In boron/titanium composites, the titanium matrix is much stronger and stiffer than an aluminum matrix. Titanium also has a higher strain to yield (typically above 0.007). Therefore, the cyclic fatigue strain of the titanium matrix is closer to that of the boron fiber than is the aluminum matrix. Because of the higher strength and stiffness of the titanium, there is a greater stress concentration in the fiber ahead of a matrix crack than would be found in an aluminum matrix composite. Therefore, in a titanium matrix composite with a strong fiber matrix interface, fatigue damage could initiate in the matrix and grow in a self-similar manner through both fiber and matrix.

These three possible fatigue failure modes in continuous fiber-reinforced metal matrix composites -- (1.) matrix dominated, (2.) fiber dominated, and (3.) self-similar damage growth -- will be covered in the remainder of the paper.

2.0 MATRIX DOMINATED FATIGUE DAMAGE

This section will consist of an introductory discussion on fatigue damage development in MMC and a philosophical approach to the problem. This discussion will be followed by a discussion on the evaluation of composite laminate shakedown limits, a review of experimentally observed fatigue damage, and a presentation of a damage development model, followed by comparisons of model predictions to experimental data.

Fatigue damage and failure of metal-matrix fibrous composites have been extensively studied in past years. Most investigations were experimental, concerned with determining S-N curves for unnotched unidirectional and laminated plate specimens [1-6], as well as evaluating crack growth rates in notched plates [7,8]. Hancock [5], in particular, gave a good review of the S-N fatigue investigations through 1974. Most of these studies dealt with boron/aluminum (B/Al) laminates. The results indicate relatively high endurance limits of 10^7 cycles, which depend on the cyclic loading conditions. Specifically, in the case of unidirectional specimens the magnitude of the 10^7 cycle endurance limit depends on the stress amplitude and is almost independent of the mean stress [9].

A simple analysis of the stress distribution in cyclicly loaded unidirectional metal matrix composites revealed that in annealed or as-fabricated B/Al specimens the matrix yielded and deformed plastically at relatively low applied stresses, but may have resumed an elastic response during subsequent cyclic loading [9,10]. In any case, the response of the matrix to sustained cyclic loading depended

on the stress amplitude and was independent of the mean stress. The local stresses supported by the elastic boron fibers depended both on the applied mean stress and the stress amplitude, and could approach about 75% of the static fiber strength even in specimens that survived more than 10^7 load cycles.

Associated studies provided some insight into the microscopic fatigue mechanisms, particularly in unnotched, unidirectional B/Al specimens. There is general agreement that important sources of fatigue cracks are isolated fiber breaks which may occur during fabrication or at the beginning of cyclic loading. These initial cracks can be attributed, in part, to the statistical variation of fiber strength and, therefore, are unavoidable. Since the boron fibers have a relatively high resistance to fatigue, additional fiber failures after first loading are apparently caused by high local stresses created in the fibers by approaching matrix cracks. However, not all matrix cracks are connected with broken fibers. White and Wright [8] observed the existence of many fatigue cracks in the matrix, some of which propagated completely through the matrix before failure of the fibers causes the composite to fail [8].

These experimental and analytical considerations lead to the conclusion that crack propagation in the matrix is the dominant event in the fatigue of B/Al composite systems. Unlike the initial fiber breaks at which cracks nucleate, fatigue crack propagation in the matrix can be avoided, or at least reduced to harmless levels by controlling the amplitude of the applied stress.

Since it is possible to view the fatigue process in terms of crack propagation mechanisms, one might hope that analytical models

describing the process can be developed for damage prediction and control. Unfortunately, the geometry of the damage state is extremely complex. Even in unidirectional specimens there , is evidence that many cracks propagate simultaneously in the matrix, sometimes at distances which are comparable to the fiber spacing. It is clear that the geometry will be even more complex in laminated structures, with different crack systems in individual laminae, interacting at, and growing along the lamina interfaces. Although there have been serious attempts to analyze such damage states in fibrous composites [11], much more effort will be required before these studies yield readily applicable results.

An alternative approach to the control of fatigue damage in MMC can be based on available information about the fatigue behavior of the metallic matrix material. Specifically, one can argue that if the cyclic stresses in the matrix do not exceed the 10^7 cycle endurance limit of the matrix material, the matrix may be able to contain the cracks initiated at fiber breaks by preventing them from spreading. This argument can be extended further in the case of the widely used aluminum matrices, in which the cyclic yield strength and high-cycle endurance limits seem to coincide [12,13]. Figure 1 illustrates this relationship which appears to hold up to relatively high levels of stress. Most annealed and as-fabricated materials will have matrix cyclic yield strengths in the range of 70-140 MPa where the relationship holds. Later a specific example of this coincidence in the case of a 6061-0 aluminum alloy will be shown. It is possible that other soft materials, such as magnesium and copper exhibit similar behavior. However, the fatigue endurance limit of some

heat-treated aluminum alloys, such as 6061-T6, is much lower than their yield strength, in which case the relationship of Fig. 1 will no longer hold.

More generally, the alternative approach to controlling fatigue damage in certain aluminum-matrix fibrous composites can be based on the argument that the initial damage will essentially be contained during 10^7 cycles of load, providing that the cyclic load amplitude is limited so that it does not cause stress levels in the matrix to be above the fatigue endurance limit of the matrix material. (For example, no sustained cyclic plastic straining of the matrix material in the case of annealed 6061 aluminum.) It is well known that elastic-plastic materials in structures subjected to variable repeated loads in the plastic range can experience failure by cyclic plastic straining or, alternatively, can shake down (i.e., resume an elastic deformation mode after a certain number of plastic strain cycles [14,15].) Methods for determining the shakedown limits (i.e., applied load amplitudes which will cause the body to shake down) have been well developed in the plasticity theory of metals [16] and also applied to fibrous composites [17].

The remainder of this section first presents an evaluation of shakedown limits in laminated plates. Next, results of tensile fatigue tests on 6061-0 B/Al unidirectional materials and several laminated plates illustrating certain microstructural aspects of fatigue damage in laminates are given. Then, a model relating the shakedown limit to stiffness loss in laminated MMC is reviewed. Lastly, the presented model is compared to experimental results.

2.1 Shakedown Limits in Fibrous MMC

The possible relationship between fatigue and shakedown in metal matrix composites was first suggested by Dvorak and Tarn [9] and related to then available experimental data, obtained primarily for unidirectional 6061 B/Al materials. In subsequent papers [18-21], the relationship was examined theoretically and experimentally for both unidirectional and laminated 6061-0 B/Al composites.

In the following text, various analytical aspects of predicting laminate shakedown, including the associated elastic-plastic behavior, will be briefly reviewed to give the reader a better understanding of the mechanics of continuous fiber-reinforced MMC. First, a material model representing lamina behavior will be presented. This will be followed by a description of the procedure used to calculate the lamina's elastic properties. Next, a lamina yield criteria is discussed, followed by a description of the matrix hardening rule. Lastly, a discussion on how the shakedown range is determined, including some example predictions is presented.

2.1.1 Material model of a unidirectional lamina

In choosing an appropriate model for construction of shakedown limits in elastic-plastic unidirectional composites, one would prefer to adopt the models which have been used with success in formulations of elastic constitutive relations, initial yield surfaces, and in solving axisymmetric plasticity and shakedown problems in fibrous composites [10,17,22]. These models were developed using a single fiber composite cylinder. For reasons explained elsewhere [23], such an approach would be impractical. Instead, it is necessary to use a

somewhat simpler material model which represents only the essential aspects of the elastic-plastic behavior.

Figure 2 shows a schematic drawing of such a model of a lamina. It consists of a matrix unidirectionally reinforced by continuous elastic fibers. The fibers are assumed to be of very small diameter, so that although they occupy a finite volume fraction of the composite, they do not interfere with matrix deformation in the transverse and longitudinal directions. As a result, the transverse tension and shear as well as longitudinal shear response of the composite are derived from the response of the matrix, except when there is an axial prestrain, and coupling of axial and transverse plastic strain components is encountered. The model can be represented by parallel fiber and matrix bars or plates with axial coupling.

2.1.2 Elastic response

The stress average for each constituent is uniquely determined from the overall stress average $\bar{\sigma}$ by

$$\sigma_f = A_f\bar{\sigma} \ , \ \sigma_m = A_m\bar{\sigma} \ , \quad v_fA_f + v_mA_m = I \tag{1}$$

where A_r (r = f, m) represents the stress concentration factor (i.e. percent of the lamina stress carried in the fiber or the matrix) , I is an identify matrix, and

$$\sigma = [\ \sigma_{11}\sigma_{22}\ \sigma_{33}\ \sigma_{12}\ \sigma_{13}\ \sigma_{23}]^T.$$

The subscripts f and m indicate the constituents; v_f and v_m are

their volume fractions such that $v_f + v_m = 1$.

Based on the model shown in Fig. 2, one can derive the following equilibrium and compatibility conditions for the material model:

Equilibrium: $$\bar{\sigma}_{33} = v_f \sigma_{33}^f + v_m \sigma_{33}^m, \qquad (2a)$$

$$\bar{\sigma}_{ij} = \sigma_{ij}^f = \sigma_{ij}^m, \text{ for } i,j = 1,2,3;\ i \neq j \neq 3.$$

Compatibility: $$\bar{\varepsilon}_{33} = \varepsilon_{33}^f = \varepsilon_{33}^m, \qquad (2b)$$

$$\bar{\varepsilon}_{ij} = v_f \varepsilon_{ij}^f + v_m \varepsilon_{ij}^m, \text{ for } i,j = 1,2,3.$$

Let E_f, ν_f and E_m, ν_m denote the elastic properties of the fiber and matrix, respectively. Since the matrix deformation is constrained by the fiber in only the axial direction, an elementary calculation leads to the following expressions for the elastic stress concentration factor, A^e_m, of the matrix:

$$A^e_m = \begin{bmatrix} a_m & 0 \\ 0 & I \end{bmatrix}, \quad a_m = \begin{bmatrix} 1 & 0 & 0 \\ 0 & 1 & 0 \\ \frac{v_f a}{E_c} & \frac{v_f a}{E_c} & \frac{E_m}{E_c} \end{bmatrix} \qquad (3)$$

where

$$E_c = v_f E_f + v_m E_m, \quad a = \nu_m E_f + \nu_f E_m.$$

The elastic stress concentration factor A^e_f can be obtained from the last of Eqs (1).

The overall elastic moduli and compliances of the composite can be determined in a similarly simple form [24].

2.1.3 Initial yielding

From the concentration factors (Eq.(3)) one can find the equation for the initial yield surface of the lamina as follows. If one assumes that the matrix obeys the Mises yield condition and that

Y is the tensile yield stress, the result is

$$f = \bar{\sigma}^T \begin{bmatrix} a_m{}^T c a_m & 0 \\ 0 & 3I \end{bmatrix} \bar{\sigma} - Y^2 = 0, \qquad (4)$$

where

$$c = \begin{bmatrix} 1 & -1/2 & -1/2 \\ & 1 & -1/2 \\ \text{sym.} & & 1 \end{bmatrix} .$$

When this yield condition is compared with more accurate results [10], one obtains good agreement for stress states which do not have a high hydrostatic component. The surface given by Eq.(4) represents an open cylinder in the generalized stress space [10] and, therefore, does not give accurate predictions of yielding for certain special axisymmetric loading directions, as discussed by Dvorak and Bahei-El-Din [22]. However, since these particular loading directions are not encountered in laminated plate structures, the yield condition in Eq.(4) is satisfactory for our present purpose.

When the lamina yield condition is used in conjunction with a simple lamination theory, one can obtain yield surfaces for each layer of the laminate and for the macroscopic laminate itself. The procedure is quite complex and details can be found in Ref.[24]. An illustration of calculated results for a specific laminate layup which has been used in the experimental work is shown in Fig. 3 . Here S_{11} and S_{22} are the overall stresses applied to the laminate in the 0^o and 90^o fiber directions, respectively, and Y is the matrix cyclic hardened yield strength in simple tension. Each layer has its own elliptical yield surface which can be found using Eq. (4). The overall yield surface of the laminate is the internal envelope of the

individual yield surfaces.

2.1.4 Hardening rule

A hardening rule describing the kinematic motion of the yield surfaces for the material model of Fig. 2 has been constructed in Refs. [23,24]. The essential feature of the hardening rule is derived from the fact that the elastic fibers can support a normal residual stress component in the fiber direction x_3 after a cycle of plastic loading and unloading by an overall stress $\bar{\sigma}_{33}$. When this residual stress is accounted for in the yield condition of Eq.(4), it appears as a translation factor causing motion of the original yield surface in the $\bar{\sigma}_{33}$ direction. Accordingly, the equation of the current load surface has the form of Eq.(4) where

$$\bar{\sigma} = [\ \bar{\sigma}_{11}\ \bar{\sigma}_{22}(\ \bar{\sigma}_{33} - \alpha\ )\ \bar{\sigma}_{12}\ \bar{\sigma}_{13}\ \bar{\sigma}_{23}]^T$$

instead of the form following Eq.(1). The evaluation of the translation vector α is outlined in Refs. [23,24] and will be omitted here. It is clear, however, that the existence of a fiber-supported residual stress causes a rigid-body translation of the initial yield surface of a lamina in the fiber direction. This aspect of composite plasticity has also been described in earlier work on axisymmetric problems [17,22].

A hardening rule for laminated plates can be developed from that for a unidirectional lamina when the stress distribution between the layers and their mutual constraints are taken into consideration. This procedure is described in Ref.[24]. Since the fibers are now

present in more than one direction, several residual stress components may exist in the matrix of each lamina, and, therefore, each of the individual yield surfaces may experience a rigid body translation in a direction which may not necessarily coincide with the local fiber direction. In other words, if for a specific lamina (i), the yield condition in Eq.(4) is written as $f_i(S) = 0$, where S is the overall stress space applied to the laminate as in Fig. 3, then the equation for lamina load surface at a particular stage of plastic loading of the laminate is

$$f_i(S - \alpha_i) = 0, \tag{5}$$

where α_i is the translation vector of the yield surface of layer (i) in the overall stress space S. Clearly, each of the local yield surfaces now can translate to any position in the stress space S which may be required by any chosen program of loading. It is equally clear that the local surfaces will not translate independently of each other. In fact, they will always tend to assume a clustered configuration with an internal envelope which will be the current yield surface, or load surface, of the laminate and will contain the current loading point.

An example of laminate hardening appears in Fig. 4. The figure shows the overall internal yield surface of a $[0/\pm45/90]_s$ B/Al laminate. The surface is similar to the one shown in Fig. 3, although now only the internal envelope (the composite yield surface) is shown. The dashed ellipse in Fig. 4 is the initial yield surface of the matrix material alone. The relatively small difference between the size of the matrix and composite yield surfaces

illustrates the well known fact that fiber reinforcement has only a small influence on the magnitude of the initial yield stress of the composite material. In addition to the composite and matrix material yield surfaces, Fig. 4 shows the current yield surface, or load surface, created during the loading from $S_{11} = S_{22} = 0$ to $S_{11}/Y = 3.0$, $S_{22} = 0$. Each of the elliptical yield surfaces constructed for the individual lamina translates as a rigid body according to its own hardening rule. The result shown is for one-half cycle of loading; a suitable loading program could be designed to cause further deformation of the current yield surface, for instance, such that the translated surface would assume a shape identical to the initial yield surface of the laminate.

2.1.5 Shakedown

According to the first shakedown theorem or Melan's theorem [14,15], an elastic-plastic body will shake down for an arbitrary program of variable repeated loads, within prescribed limits, if any time-independent state of residual stress can be found such that the superposition of this state and the elastic response for all possible combinations of external forces within the prescribed limits will not lead to stresses at or above yield at any point [15,16]. It is self-evident that the initial yield surface, or any subsequent load surface, represents a lower bound on the shakedown limits of the structure.

If fatigue damage in general is to be avoided, and low cycle fatigue failures in particular, the cyclic loading must produce only elastic strains in the constituents. Even so, local plastic

straining can be permitted in the composite during the first few load cycles, provided that the composite "shakes down" during these few cycles. The shakedown state is reached if the matrix cyclically hardens to a cyclic yield stress Y such that, subsequently, only elastic deformation occurs under load cycles. The shakedown limit for the composite containing 0^{o} fibers is considerably below the composite's fatigue limit.

The shakedown stress range for a unidirectionally loaded laminate can be found using laminate theory to determine the yield surface for the individual plies in the laminate. As described earlier, Fig.3 shows an example of a $[0/\pm 45/90/0/\pm 45/\overline{90}]_s$ lay-up under biaxial inplane stresses S_{11} and S_{22}. Each ply has its own elliptical yield surface, constructed analytically from the ply matrix stresses and the von Mises yield condition. The overall yield surface of the laminate is the internal envelope of the yield surfaces of the individual plies. The shakedown stress range, S_{Sh}, is the width of the overall yield surface in the S_{11} loading direction. The value of ΔS_{Sh} can be calculated easily with an computer analysis AGLPLY, briefly described in Ref.[24]. AGLPLY uses the composite constituent's properties as input and calculates the laminate properties using the micromechanics assumptions described earlier.

In concluding this section, we list the composite constituents' mechanical properties in Table 1 and the magnitudes of the shakedown stress range, ΔS_{Sh}, in Table 2 for materials which have been used in the experimental programs reported in Refs.[21,26]. Also included in Table 2 is the initial (undamaged) elastic modulus E_0 of each

laminate. In each case we consider material loading in the 0^{o} fiber direction and the material properties shown in Table 1.

2.2 Fatigue Damage

In this section we will review the experimental data on annealed 6061 aluminum, boron/aluminum (B/Al) and silicon-carbide/aluminum (SiC/Al) composites from references [18-21,25,26]. The aluminum matrix in each laminate is annealed 6061 aluminum. Micrographs of typical matrix dominated fatigue data will be shown. Data will be presented to illustrate how the matrix damage effects the stiffness of the laminate.

Previous tests have shown that the matrix fatigue limit coincides with the stable cyclic yield stress for annealed aluminum [12,13,25] and steels [13]. The value of Y is 70 MPa for annealed 6061 aluminum [18,25]. Fatigue S-N data for 6061-T0 (annealed) is shown in Fig.5. Notice that the S-N data lie on a curve that is essentially flat. If cycled below the elastic stress range (2Y=140 MPa), the specimen lasts over two million cycles. If cycled above 140 MPa, the life is much shorter.

When specimens were cycled above their shakedown range, matrix cracks were observed [25]. The specimens were then optically examined for fiber failure and matrix cracking after gradual etching of the surface layer of aluminum matrix in a 30 percent hydrochloric acid (HCL) solution of distilled water. Fiber failure was detected only in specimens subjected to stresses that approached the fatigue limit. However, substantial changes in the laminate modulus were detected well below this stress level. Those specimens that

sustained modulus loss without laminate failure had long matrix cracks which grew parallel to the fibers in the off-axis plies of the laminate. Limited cracking perpendicular to the loading direction was observed in the matrix of the 0^{o} plies when cycled near the fatigue limit [8,19]. (Notice that in Fig. 3 the 45^{o} and 90^{o} plies yield at a lower laminate stress than the 0^{o} plies; therefore, the matrix in the off-axis plies would be expected to undergo more plastic deformation, which, in turn, would lead to more fatigue cracking than in the 0^{o} plies. Indeed, the off-axis plies were observed to have more cracks.) These cracks appeared to be mostly within the individual off-axis plies. The individual cracks did not extend into adjacent plies of different ply orientations. No delamination was found between the plies, as is commonly reported for polymer matrix composites. (The lone exception was the SiC/Al laminate [26]. Delamination there was caused by very weak fiber/matrix interfaces.) Since cracks in the matrix of the off-axis plies were the only observed damage of consequence, almost all of the observed modulus decreases are likely to be attributable to these cracks. Figure 6 shows a photomicrograph of cracks in the matrix of a 45^{o} ply of a B/Al laminate. Figure 7 shows the matrix cracks in the 90^{o} ply of a $[0/90]_{2s}$ laminate. Similar matrix cracking was found in SiC/Al composite laminates, as well as, edge delaminations due to poor fiber/matrix bonding [26].

These matrix cracks reduce the effective tensile modulus of the matrix. The cracks also tend to open and close under remotely applied cyclic loads. This matrix cracking and subsequent crack opening and closing result in a bilinear response, (explained later

in the paper) which may be observed from experimental stress-strain responses, as shown in Fig. 8 for the 500 000th cycle. The amount of damage (matrix cracking) can be inferred from the changes in the elastic unloading modulus E_N [18,25]. The elastic unloading modulus E_N, shown in Figure 8, is a reliable measure of fatigue damage in a MMC laminate because it is a function of only the constituent moduli. So, if fibers break or the matrix cracks, E_N will decrease. The laminate stiffness (secant modulus E_S) is a poor indicator of laminate damage because it is a function of matrix yield strength. The stiffness actually increases as the matrix cyclically strain hardens during fatigue and decreases due to laminate fatigue damage [25]. (Earlier, Stinchcomb, et al.[27], showed similar stiffness changes with cycling of B/Al laminates containing circular holes.) Stress-strain data were taken at intervals during the fatigue cycling to record the change in the laminate modulus as a function of the number of cycles. The damage was expressed in terms of its effect on E_N normalized by E_0 , the initial elastic modulus of the first cycle. An example of the fatigue damage accumulation as a function of the number of applied cycles and stress level is presented in Fig.9 for a $[0/\pm45/90/0/\pm45/\overline{90}]_S$ laminate. Most of the damage (as indicated by the change in E_N/E_0) occurred in the first 500 000 cycles. Notice that each specimen appeared to reach a stabilized value of E_N/E_0, herein referred to as a saturation damage state (SDS). After the saturation damage state is reached, a laminate will neither accumulate more damage nor fail under the present loading condition.

Returning to Fig. 8, the cyclic stress-strain curve for the fourth cycle includes elastic and plastic deformation and has a

secant modulus E_S of 10.82×10^4 MPa. For the same specimen, the 500000th cyclic stress-strain curve has a very different shape with an associated secant modulus of 8.88×10^4 MPa. The change in the shape of the stress-strain curve and the drop in secant modulus (almost 22%) are attributed primarily to matrix cracking. In contrast, hardening of the matrix material usually causes the secant modulus to increase after some initial cycling. Notice that, due only to plasticity, the fourth cycle in Fig.8 has a secant modulus much smaller than the elastic modulus (Table 2). If the laminate was cycled at or below the shakedown range, the matrix would harden so that the secant modulus would be approximately equal to the elastic modulus.

2.3 Matrix Damage Model

A simple analysis was developed to predict the decrease in laminate secant modulus caused by matrix damage [21]. The model starts with the matrix cycling plastically. As cracks develop due to plastic cycling, the effective modulus is reduced for the portion of the matrix cycle that is in tension. The model presents simple equations to approximate the effective matrix modulus due to cracking at an assumed cyclic strain range. The program AGLPLY [24] is used to calculate the laminate response with the effective modulus of the fatigued matrix. Thus a bilinear response, such as shown in Fig. 8, can be computed. The secant modulus is calculated from the bilinear response.

Figure 10 illustrates this behavior in terms of the applied laminate stress and the corresponding axial stresses in the matrix

and 0^o fibers. The dashed lines in Fig.10 represent the initial loading response. Accordingly, the first load cycle causes the matrix and 0^o fiber stresses to follow the dashed loops. , The laminate has an ideally elastic-plastic matrix (for illustration of the model and simplicity of presentation) and is subjected to a constant cyclic stress range, ΔS. The dashed loops are for the same condition represented in Fig. 8 in the fourth cycle. σ_{Sh}^m is assumed to be the axial stress in the matrix material in the loading direction at the shakedown stress limit ΔS. (The matrix is yielded at this point by a combination of axial and shear stresses.) Assuming the matrix yields at the same value in tension and compression, σ_{Sh}^m equals half of the laminate's shakedown strain range $\Delta S_{Sh}/E_0$ times the matrix tensile modulus, E^m.

$$\sigma_{Sh}^m = \Delta S_{Sh}/2E_0 \times E^m \qquad (6)$$

The ΔS_{Sh} in this equation is the shakedown stress range, E_0 is the undamaged laminate's elastic modulus in the loading direction, and E^m is the undamaged matrix's elastic modulus. With subsequent cycling, the cyclic plasticity causes matrix cracks to initiate and grow, effectively decreasing the matrix tensile modulus until a saturation damage state is reached. The dashed loops in Fig.10 narrow to zero-width loops shown as solid lines, which represent the saturation damage state. These solid lines correspond to the laminate cyclic stress-strain response illustrated in Fig. 8 for the 500 000th cycle. The saturation damage state develops when the matrix cracking causes the load to transfer to the 0^o fibers, thus relieving the matrix from undergoing additional damaging plastic deformation.

The drop in matrix modulus in the load direction due to fatigue damage can now be determined using Fig.11. The strain in the matrix and laminate is plotted versus the matrix stress σ^m or the laminate stress S. The damage state has an associated cyclic strain range, $\Delta\varepsilon$. If this cyclic strain range is assumed, an effective tensile modulus of the matrix material E^m_{eff} can be estimated. This assumes that the same SDS will be reached by either stress or strain control. Note that E^m_{eff} is the modulus in the loading (0^o fiber) direction. The compressive strain range of the matrix $\Delta\varepsilon^m_{comp}$ was approximated as

$$\Delta\varepsilon^m_{comp} = \Delta S_{Sh}/2E_0. \qquad (7)$$

The effective tensile modulus of the matrix material can now be approximated by dividing σ_{Sh}^m by the cyclic strain minus the compressive portion.

$$E^m_{eff} = \sigma_{Sh}^m/(\Delta\varepsilon - \Delta\varepsilon^m_{comp}) \qquad (8)$$

E^m_{eff} is used as the matrix modulus in lamination theory (using the computer program AGLPLY) to calculate E_{SDS}, the unloading elastic modulus of the composite in its saturation damage state (at approximately 500 000 cycles). The shear modulus of the matrix is also reduced within AGLPLY based on E^m_{eff} and Poisson's ratio. All the fibers were assumed to be intact, and the matrix damage was assumed to be characterized by the laminate's lowered modulus, E^m_{eff}. Although such a formulation implicitly assumes that the matrix modulus is reduced isotropically, the reduction actually is

orthotropic. However, the interest is in the laminate modulus in the primary loading direction only, and the assumption should not introduce excessive error.

Returning to Fig.11, we now know the modulus for each of the two linear segments, as well as the strain ranges. Therefore, the overall laminate stress range ΔS can be calculated as follows

$$\Delta S = (\Delta \varepsilon^{m}_{comp}) E_0 + (\Delta \varepsilon - \Delta \varepsilon^{m}_{comp}) E_{SDS} \qquad (9)$$

Equation (9) is rewritten using Eq (7).

$$\begin{aligned} \Delta S &= E_{SDS} \Delta \varepsilon + 1/2 \, \Delta S_{Sh}(1 - E_{SDS}/E_0) && \text{for } \Delta S > \Delta S_{Sh} \\ &= E_0 \Delta \varepsilon && \text{for } \Delta S \leq \Delta S_{Sh} \end{aligned} \qquad (10)$$

The values of ΔS_{Sh}, E_0, and E_{SDS} were calculated using AGLPLY. Equation (9) applies to either stress- or strain-control cycling. By selecting a number of different strain range values $\Delta \varepsilon$, the corresponding laminate stress range ΔS can be calculated and plotted versus $\Delta \varepsilon$. The laminate secant modulus then is

$$E_S = \Delta S / \Delta \varepsilon \ . \qquad (11)$$

2.4 Comparison Of Model To Data

Experimental data are now taken from the literature and compared with the presented model to test the shakedown theory. The data has been divided into three groups because of their basic differences in damage development and growth. The first group examined are unnotched laminates containing 0^{o} plies. The second group consists of unnotched $[\pm 45]_{2s}$ laminates. The last group consists of laminates

containing notches (both holes and slits will be discussed).

2.4.1 Laminates Containing 0^o Plies

The predicted cyclic stress-strain response after 500 000 cycles and the associated secant modulus are presented in this section and compared with measured experimental results [21]. The predictions are shown as solid lines (see Fig.12 as an example). For reference, a dashed line representing the undamaged elastic modulus of the laminate is shown. The secant modulus scale can be read in two ways. First, entering on the ΔS axis, crossing to the solid prediction line and down to the secant modulus scale gives the secant modulus of a laminate after 500 000 cycles at a given stress range. Second, one can drop from the cyclic strain scale directly to the secant modulus scale to assess the secant modulus after 500 000 cycles at a given strain range. Notice that the secant modulus scale is nonlinear. Also notice that the secant modulus scale ends on the left at the shakedown limit; the secant modulus is equal to E_0 below the shakedown limit. The experimental data were generated at stress ratios R between 0.0 and 0.5. Since the data showed little scatter, this confirmed that the damage developed in the matrix is a function of stress range ΔS and not of R (or mean stress).

Figures 12 through 16 present some of the experimental and analytical correlation of B/Al laminates from Ref. [21]. Figures 17 and 18 present SCS_2/Al laminate data from Ref. [26]. SCS_2 is a silicon-carbide fiber made for aluminum matrix applications by AVCO Specialty Materials Division of Lowell, MA.

Figures 14 and 15 present data for the $[0_2/\pm45]_s$ and $[0/\pm45]_s$

B/Al laminates, respectively. These tests are significant because they were conducted under both stress and strain control. The experimental data indicate that the same damage state is reached whether the stress is held constant and the strain increases or the strain is held constant and the stress decreases. This material behavior allows one to assume a constant strain range to calculate fatigue damage for strain or stress control tests in the presented analysis.

Figures 13 and 16 include data points representing the initial cyclic response of the laminate (for example, the fourth cycle in Fig. 8). These data illustrate the secant modulus loss due to matrix yielding. The initial cyclic stress-strain responses are reasonably close to the predicted response after 500 000 cycles; however, as shown in Fig. 8, the reason, or mechanism, for the secant modulus loss is different.

Figures 13 and 14 show that stacking sequence has very little effect on the secant modulus E_S in $[0/90]_{2S}$ - $[90/0]_{2S}$, and $[0_2/\pm45]_S$ -$[\pm45/0_2]_S$ laminates, respectively. Previous research [1] showed that the stacking sequence may have an effect on the degradation of the elastic unloading modulus E_N, in particular, near the shakedown limit [20,25].

Figures 17 and 18 show good correlation between the model and test data for $[0]_8$ and $[0_2/\pm45]_S$ layups of SCS_2/Al composites [26], respectively.

In general, the shakedown damage model predictions fit the experimental data very well even though the individual data points were generated at different stress ratios. This confirms the

observation [9,25] that the matrix damage is a function of stress range and not mean stress. The data fell slightly above the predictions in some cases and slightly below in others. Some of this scatter may be attributed to deviations in the fiber volume fraction from what was assumed. Also, the annealing treatment of the aluminum matrix may have varied from one laminate to another. It is also acknowledged that the assumption of isotropically decreasing the modulus of the matrix due to cracking may affect the predicted results for various laminates differently. In any case, the present model does a very good job of representing the extent of accumulated fatigue damage in the saturation damage state and predicting the observed material response.

2.4.2 $[\pm 45]_{2S}$ Laminates

The $[\pm 45]_{2S}$ SCS_2/Al laminate data [26] presented in Fig. 19 is unique among the laminates tested since it has no 0^o fibers to carry the load from the damaged matrix as suggested in the previously discussed shakedown stiffness loss model.

Below the shakedown stress range of 150 MPa, shown in Fig.19, the specimen underwent large plastic deformations (as much as 0.08 strain). Also, during cyclic loading, the matrix yield stress changed from its initial value of 40 MPa to a fully hardened, stabilized value of 150 MPa. The rotation of fibers (to approximately $\pm 41^o$) actually caused the elastic modulus and secant modulus to increase slightly. The cross-sectional area of the specimen decreased by approximately 8% during a cyclic stress range of 138 MPa. The stress-strain behavior of the laminate stabilized. No fatigue damage

was noticed.

Above the shakedown stress range, fatigue damage developed in the $[\pm 45]_{2S}$ laminate in the form of many matrix cracks growing into the specimen from the edge. Under these conditions, the elastic modulus and the secant modulus of the laminate decreased. At ΔS=172 MPa the fibers rotated to $\pm 39^{o}$. Once fatigue damage initiated in the matrix it eventually grew to cause laminate failure since there were no 0^{o} fibers to carry the load in a strain controlled fashion. Thus, the fatigue limit of laminates containing no 0^{o} fibers may be estimated by the shakedown stress range.

2.4.3 Laminates Containing Holes or Slits

Grimsley [28] used the previously discussed shakedown model along with a stress analysis of a pin loaded hole joint to predict the loads at which joint specimens would fail in fatigue. Failure was defined as a 1.27 mm elongation of the hole as measured by the pin deflection. Specimens were made of B/Al, SiC/Al, or B_4C/Al (borsic fiber reinforced aluminum). One joint specimen, which was predicted not to fail in fatigue based on shakedown theory, did not fail after five million constant amplitude fatigue cycles. Other joint specimens were fatigued above the calculated shakedown limit at the edge of the hole and failed within a half million cycles. This limited amount of data supports the use of the shakedown theory for predicting local damage around notches.

Saff [29] has additional data to support this approach for aluminum matrix MMC with holes. Figure 20 shows the relative effect of the matrix yield strength, matrix fatigue, and fiber fatigue for

an unidirectional B/Al specimen containing a filled hole. Note that when the stress level is too low to cause matrix yielding (less than 30% ultimate tensile strength), the lives to crack initiation (represented by a 1.27 mm long crack) are very long. As the load levels increase, lives to crack initiation decrease but the fiber stresses will not cause failure. At loads levels above approximately 75 percent of the ultimate, fiber failure begins to control the life. These failures can occur at such short lives that matrix cracks will not develop before failure.

Saff [29] also reported that when notched unidirectional B/Al specimens are fatigued at stress levels above matrix yield but below fiber failure, cracks initiated in the matrix at the notch tip and grew parallel to the fibers. These cracks were driven by shear in the matrix. This matrix shear stress was a constant driver since the flaw growth did not affect the net section or other geometrical parameter. This constant driving force was reflected by nearly constant crack growth rates measured experimentally.

Simonds [30] fatigued several different B/Al laminates containing centered crack-like slits. The fatigue load was high enough to cause damage at the end of the slit but low enough not to cause laminate failure in 100 000 cycles. Some specimens were radiographed and others were sectioned and examined microscopically to determine the extent of fatigue damage in terms of fiber failures and matrix cracking. Many split or broken 45^{o} fibers were found at the slit tip. This reflects the low transverse strengths of the boron fibers as reported by Johnson, Bigelow, and Bahei-El-Din [31]. Considerable matrix cracking was found in the 45^{o} plies at the slit

tip. In those specimens containing at least 50% 0^o plies, matrix cracks in the 0^o direction were found at the slit tip growing parallel to the fibers toward the grips. Since the fatigue levels chosen ranged from 25 to 50% of the static ultimate stress for the unidirectional specimens and from 50 to 80% for those specimens with cross plies, broken 0^o fibers were seldom found at the slit tip. Therefore, the fatigue damage had a negligible effect on the residual static strength which is primarily a function of the 0^o fibers.

2.5 Summary of Matrix Dominated Damage

Matrix damage can affect the laminate stiffness properties significantly. For unnotched specimens, the resulting secant modulus after 500 000 cycles is significantly below the elastic modulus for all of the tested laminates, except the $[0]_8$ laminates. If compared at a cyclic strain range of 0.004, the $[0]_8$ laminate retained approximately 95% of the original elastic modulus. The other laminates retained about 60 to 70% of their original moduli. These differences between the often calculated elastic modulus and the resulting secant modulus must be addressed by the designers of stiffness critical parts. Certainly, the unidirectional laminate may still retain the desired stiffness, but laminates with off-axis plies must be scrutinized for their design load levels and stiffness requirements.

The results presented for matrix dominated fatigue damage indicate the existence of three distinct regions in the S-N plane in which one observes different responses of MMC to cyclic loading. Figure 21 illustrates these regions for a $[0/\pm45/90/0/\pm45/\overline{90}]_S$ B/Al

laminate. At low stress levels, below the shakedown stress limit (218 MPa), there is no significant accumulation of fatigue damage. The elastic modulus and static strength remain intact up to, and probably beyond, two million cycles. Above the shakedown stress level there is a damage accumulation region, where reductions in the elastic modulus are observed after a certain number of cycles. The S-N curve is a boundary between the damage accumulation region and the fracture region. Graphs, similar to Fig.21, can be constructed for other laminates and material systems and would be useful for designing MMC components.

If a designer only concerned himself with the materials S-N fatigue behavior shown in Fig. 21, he would chose 70% of ultimate as a safe design load for a life up to at least 2 million cycles. However, the MMC would experience a significant loss of stiffness. If the designer wished to retain all of the initial stiffness for the 2 million cycle lifetime, then he should not allow the cyclic stress range to exceed 35% of ultimate for this particular composite.

The presented results also indicate that matrix damage at notch tips can be predicted using the shakedown criteria. Similar matrix damage takes place on a local scale at the notch tip.

3.0 FIBER DOMINATED FATIGUE DAMAGE

Tsangarakis, Slepetz, and Nunes [32] investigated the fatigue behavior of two different batches of an alumina fiber reinforced aluminum composite (FP/Al). This section will essentially be a review of their work. Both batches that they tested had a nominal fiber volume fraction of 55% with the fibers uniaxially oriented in the loading direction. Tension-tension fatigue tests were conducted on flat, untabbed, contoured specimens at R=0.1. Some specimens were strain gaged so that the load-strain response could be monitored during the fatigue tests. Metallographic and fractographic examinations of the specimens were conducted to evaluate failure modes and damage mechanisms.

Fig. 22 presents fatigue data that show a significant difference in mechanical properties of the two batches of FP/Al investigated. The first batch had an endurance limit (as indicated by the runout data points) of 410 MPa compared to 330 MPa for the second batch. The static strength and modulus were correspondingly higher for the first batch than the second. Fatigue cycling did not cause a decrease of secant modulus in either batch of material, contrary to the reported behavior for B/Al. Fiber failure was found to dominate the fatigue life of FP/Al, and failure of the composite generally occurred after a sufficient number of fibers fractured at a given cross section.

The most significant damage in both failed and runout specimens of FP/Al was extensive fiber fracture, including multiple fractures of individual fibers. Even though many of the fibers were broken, some in several places, they were able to pick-up and carry load very

effectively. This is evident from the fact that the secant modulus remained essentially unchanged until just prior to laminate failure despite considerable fiber fracture. This implies that the matrix and fiber remained well bonded.

The difference in the fatigue behavior of FP/Al and B/Al is due to the differences in fiber properties. The failure strain for boron fibers is over three times that of the alumina fibers. Their respective fatigue strengths have perhaps the same ratio. On the other hand, the shakedown stress range is nearly equal for the two systems because both have essentially the same matrix yield strength and composite modulus. Therefore, fatigue failures can occur in the fibers of the FP/Al composite at stress levels below the shakedown range defining the threshold level for matrix fatigue. The larger and stronger boron fibers have greater resistance to crack propagation and deflect the crack along the fiber/matrix interface in B/Al. This results in a very erratic crack path (not flat), featuring some debonding and fiber pullout prior to fatigue failure. In the FP/Al composite, the combination of weaker, smaller diameter fibers and a stronger interface make it easier for a fatigue crack to propagate across fibers on a relatively flat plane as shown in Fig. 23.

In summary, progressive fiber fracture was found to be the dominant damage mechanism controlling the fatigue behavior of FP/Al. Once a sufficient number of broken fibers developed at a cross section, composite failure occurred.

4.0 SELF-SIMILAR FATIGUE DAMAGE GROWTH

Titanium matrix MMC are very attractive because of their high stiffness and high temperature capabilities. Ti-6Al-4V has an elastic modulus of 110 GPa. Thin sheet (1.60 and 3.18 mm) Ti-6Al-4V has a tensile yield strength of 1089 MPa [33]. This implies a strain to yield of approximately 0.01. This strain is well above the strain to failure of boron or silicon-carbide fibers. However, the fatigue endurance limit at 10^7 cycles for titanium is approximately 600 MPa [33]. In this case, the strain to the matrix fatigue limit is close to the fiber failure strain. Since the fatigue limit is significantly lower than the yield stress, the matrix may develop fatigue cracks without yielding the matrix globally. Furthermore, the titanium is much stronger than the typical aluminum matrix material, and is therefore capable of creating a much higher stress concentration in a fiber ahead of a matrix crack.

Considering the closeness of the strains for failure of the matrix and fiber and the high stress concentration capabilities of the titanium, it is not surprising that Saff and Grimsley [34] reported self-similar crack growth for notched boron/titanium (B_4C/6-4 titanium) subjected to fatigue loadings. (They also reported that in some cases fibers failed before the matrix under fatigue loading.) Saff [29] reported that the crack growth in titanium MMC was often self-similar as in metals. A comparison of crack growth rate data from center cracked panels of the MMC and the parent matrix material (Figure 24) indicates that the MMC requires higher loads to reach threshold, and provides much slower crack growth rates throughout the life. However the figure also shows that

the MMC has a lower fracture toughness. Saff felt that the higher thresholds are controlled by the fiber/matrix interface strength (the lower the interface strength, the higher the threshold) because the matrix can not transfer crack tip strains to the fiber when the interface is weak.

Saff also suggests that the overall crack growth is controlled by the fiber/matrix interface and the fiber spacing. He found examples of bundles of fibers inhibiting crack growth in the titanium MMC. The bundles essentially halted the crack growth across the fibers and forced the crack to grow parallel to the fibers until weaker fiber sections allowed the crack growth to continue across the fibers again. This process may cause an apparent acceleration in crack growth when the fiber bundle fails and releases energy into the matrix once again. The ability of the crack to change paths depends on the crack length and the fiber/matrix interface strength.

Another explanation for the slower crack growth rate of the titanium MMC shown in Fig. 24 is offered herein. The crack growth failure surface is seldom perfectly flat. Most surfaces will have at least a small amount of fiber pull-out. In addition there may well be some fractured fiber fragments embedded in the surface. This may prevent the crack from closing as fully as the parent material alone would. This results in a debris (or surface roughness) induced closure phenomenon [35] that essentially causes the crack growth rate to slow down.

In summary, self-similar crack growth may be expected in laminates that have very strong matrix materials with either of the following two conditions: (1) The strain to fatigue failure in the matrix is close to the strain required to fail the fiber; or (2) the matrix and the fiber/matrix interface are sufficiently strong to enable a matrix crack stress concentration to fail the fibers.

5.0 SUMMARY

Fatigue of metal matrix composites can be quite complex. The matrix, because of its relatively high strength and stiffness compared to the fiber, plays a very active role compared to a polymer matrix. Fatigue damage in a metal matrix can reduce the laminate stiffness by as much as 50% without causing laminate failure.

Although the elastic-plastic behavior of the metal matrix adds some complexity to the stress analysis problem, to some extent, it simplifies the fatigue problem. The understanding of fatigue behavior of metals is quite good and can be applied directly to the composite matrix. One knows, for example, that continued cyclic plasticity will cause low cycle fatigue. Therefore, if fatigue damage to the matrix is to be avoided, then so must cyclic plasticity. The composite can, therefore, be allowed to shake down and then continue to cycle elastically for a long fatigue life of the matrix. This is, of course, providing that the fatigue strength of the matrix material is equal to the cyclically hardened yield strength. If not, then, of course, the matrix stresses must be restricted to the level of the fatigue strength of the matrix material.

As presented in this paper, the fatigue failure modes in continuous fiber reinforced metal matrix composites are controlled by the three constituents of the system: fiber, matrix, and fiber/matrix interface. The relative strains to fatigue failure of the fiber and matrix will determine the failure mode. If the matrix requires much less cyclic strain to fatigue than the fiber, then the composite will be matrix damage dominated. Large losses in laminate stiffness may

result without laminate failure, as shown for B/Al and SiC/Al composites. If, on the other hand, the fiber requires less cyclic strain to fail than does the matrix, the composite will be fiber damage dominated. This composite will fail rather suddenly in fatigue with little warning, provided the fiber/matrix interface is strong enough to transfer load into the broken fibers, as shown for FP/Al. Lastly, if both the fiber and matrix require approximately the same cyclic strain for fatigue failure and the fiber/matrix interface is sufficiently strong, self-similar crack growth, as found in metals, may result as shown for B/Ti composites. Self-similar crack growth is also possible when the matrix is strong enough to create a high stress concentration in the fiber ahead of the matrix crack. Thus, by starting the fatigue damage in the matrix, the crack can propagate across the fibers.

As new continuous fiber-reinforced metal matrix composites are hypothesized and developed, projections of their fatigue behavior can be made by understanding the relative strengths of the fiber, matrix, and the fiber/matrix interface.

6.0 ACKNOWLEDGEMENT

The author would like to acknowledge Mr. C. R. Saff of McDonnell Aircraft Company and Dr. N. Tsangarakis of the Army Materials Technology Laboratory for their help in the preparation of this paper.

7.0 REFERENCES

[1] A. A. Baker, Journal of Material Science 3 (1968) 412-423.

[2] A. A. Baker, D. M. Braddick and P. W. Jackson, Journal of Material Science 7 (1972) 747-762.

[3] I. J. Toth, ASTM-STP 460 (1969) 236-253.

[4] G. D. Menke and I. J. Toth, The Time-Dependent Mechanical Behavior of Metal Matrix Composites, AFML-TR-71-102, Air Force Materials Laboratory, September 1971.

[5] J. R. Hancock, in Composite Materials, Vol 5: Fracture and Fatigue,ed. L. Broutman and R. H. Krock, Academic Press (1974) 370.

[6] J. L. Christian, ASTM STP-569 (1975) 280-294.

[7] D. P. Kendall, ASTM STP-636 (1977) 47-56.

[8] M. K. White and M. A. Wright, Journal of Material Science 14 (1979) 653-662.

[9] G. J. Dvorak and J. Q. Tarn, ASTM STP-569 (1975) 145-168.

[10] G. J. Dvorak, M. S. M. Rao, and J. Q. Tarn, Journal of Applied Mechanics 4 (1974) 249-253.

[11] A. L. Highsmith and K. L. Reifsnider, ASTM STP-907 (1986) 233-251.

[12] Aluminum, Vol 1, K. R. Van Horn, ed., American Society for Metals, Metals Park, Ohio (1967) 183.

[13] M. T. Weng, International Journal of Fatigue 3 (1981) 187-193.

[14] E. Melan, Ingenieur-Archiv 9 (1938) 116.

[15] P. S. Symonds, Journal of Applied Mechanics 18 (1951) 85.

[16] G. Maier, Meccanica 4 (1969) 250.

[17] J. Q. Tarn, G. J. Dvorak and M. S. M. Rao, International Journal of Solids and Structures 11 (1975) 751-764.

[18] G. J. Dvorak and W. S. Johnson, International Journal of Fracture 16 (1980) 585-607.

[19] G. J. Dvorak and W. S. Johnson, 1981 Advances in Aerospace Structures and Materials, ASME AD-01, New York, (1981) 21-34.

[20] W. S. Johnson, ASTM STP-775 (1982) 83-102.

[21] W. S. Johnson, ASTM STP-813 (1983) 160-176.

[22] G. J. Dvorak and Y. A. Bahei-El-Din, Journal of the Mechanics and Physics of Solids 27 (1979) 51-72.

[23] G. J. Dvorak and Y. A. Bahei-El-Din, Proc. Reseach Workshop on Mechanics of Composite Materials, Duke University, Oct 17-18, 1978.

[24] Y. A. Bahei-El-Din, Plastic Analysis of Metal Matrix Composite Laminates,Ph.D. Dissertation, Duke University (1979).

[25] W. S. Johnson, Characterization of Fatigue Damage Mechanisms in Continuous Fiber Reinforced Metal Matrix Composites, Ph.D. Dissertation, Duke University (1979).

[26] W. S. Johnson and R. R. Wallis, ASTM STP-907 (1986) 161-175.

[27] W. W. Stinchcomb, K. L. Reifsnider, L. A. Marcus, and R. S. Williams, ASTM STP-569, (1975) 115-129.

[28] F. M. Grimsley, Static and Fatigue Behavior of Pin-Loaded Metal Matrix Joints, AFWAL-TR-84-3063, Air Force Wright Aeronautical Laboratories, 1984.

[29] C. R. Saff, Durability of Continuous Fiber Reinforced Metal Matrix Composites, AFWAL-TR, Air Force Wright Aeronautical Laboratories, 1987.(in preparation)

[30] R. A. Simonds, Residual Strength of Five Boron/Aluminum Laminates with Crack-Like Notches After Fatigue Loading, NASA CR 3815, National Aeronautics and Space Administration, July 1984.

[31] W. S. Johnson, C. A. Bigelow, and Y. A. Bahei-El-Din, Experimental and Analytical Investigation of the Fracture Processes of Boron/Aluminum Laminates Containing Notches, NASA TP 2187, National Aeronautics and Space Administration, 1983.

[32] N. Tsangarakis, J. M. Slepetz and J. Nunes, ASTM STP-864 (1985) 131-152.

[33] P. E. Ruff, Metrification of MIL-HDBK-5C, AFWAL-TR-80-4110, Air Force Wright Aeronautical Laboratories, 1980.

[34] C. R. Saff and F. M. Grimsley, Testing Technology of Metal Matrix Composites, ASTM STP (1987).(in press)

[35] N. Walker and C. J. Beevers, Fatigue of Engineering Materials and Structures, 1 (1979) 135-148.

TABLE 1 - Composite constituent mechanical properties.

	Boron Fiber [21]	Silicon-Carbide Fiber [26]	6061 Aluminum
Elastic modulus,GPa	400	340	72.5
Poisson's ratio	0.13	0.25	0.33

TABLE 2 - Dimensions and properties of MMC

Laminate	v_f	Width, mm	Thickness, mm	Calculated E_0,GPa	Calculated ΔS_{Sh},MPa
B/Al [21]					
$[0]_8$	0.45	12.70	1.47	220.0	459
$[0/90]_{2s}$	0.50	12.70	1.37	184.4	220
$[90/0]_{2s}$	0.50	12.70	1.37	184.4	220
$[0_2/\pm45]_s$	0.44	18.38	1.49	170.0	216
$[\pm45/0_2]_s$	0.44	18.38	1.49	170.0	216
$[0/\pm45]_s$	0.45	18.38	1.11	157.0	195
$[0/\pm45/90/0/\pm45/\overline{90}]_s$	0.45	12.70	2.64	151.3	192
SiC/Al [26]					
$[0]_8$	0.44	19.00	1.60	190.0	368
$[0_2/\pm45]_s$	0.44	19.00	1.60	154.0	199

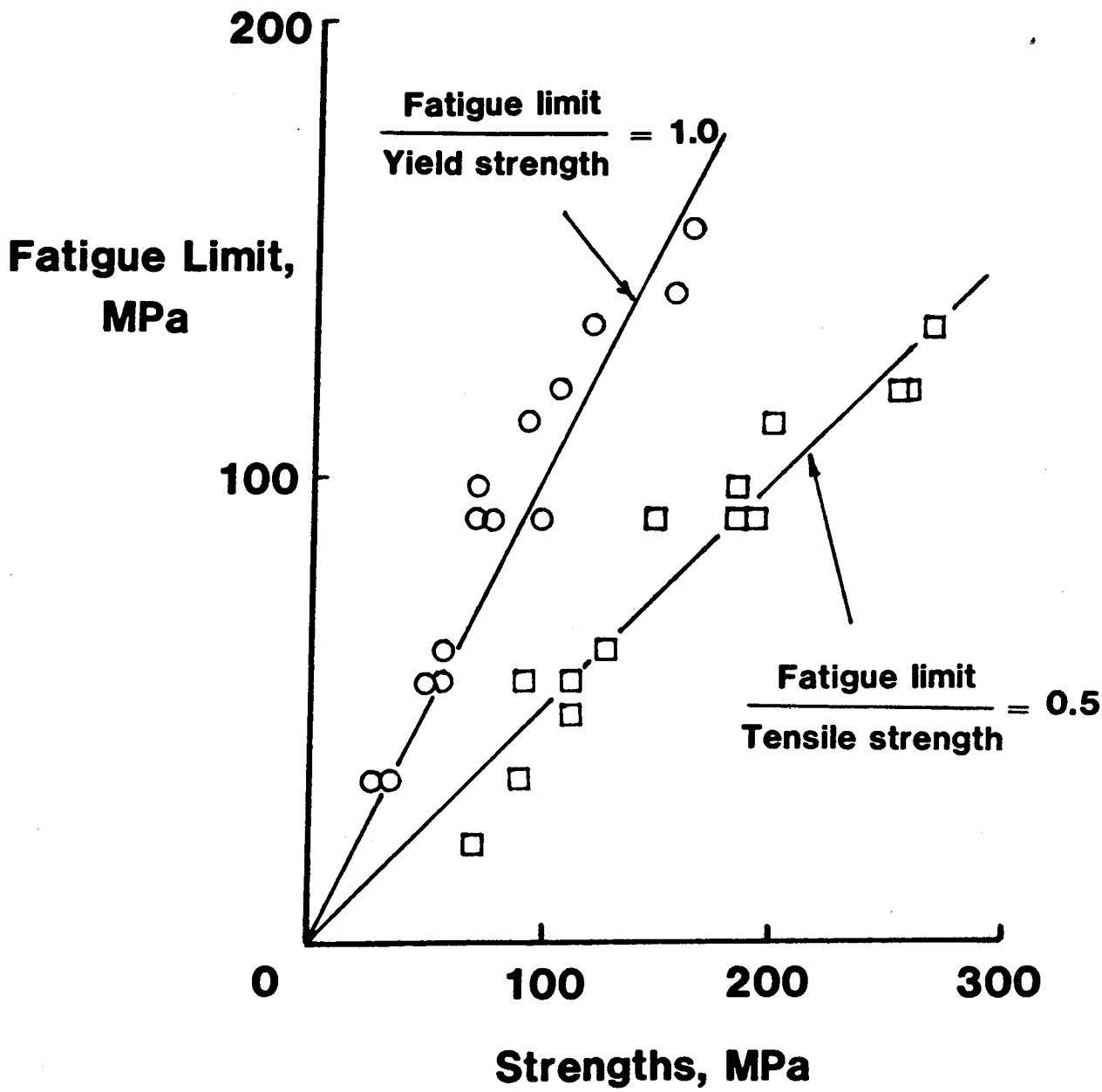

Figure 1. Relationship between 10^7 endurance limit and yield strength of certain annealed aluminum alloys [12].

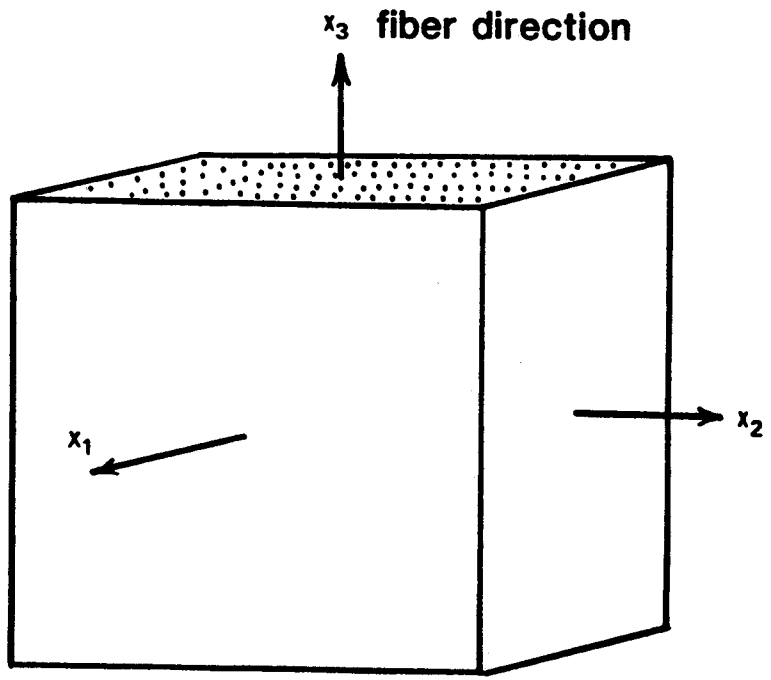

Figure 2. Material model for the elastic-plastic lamina.

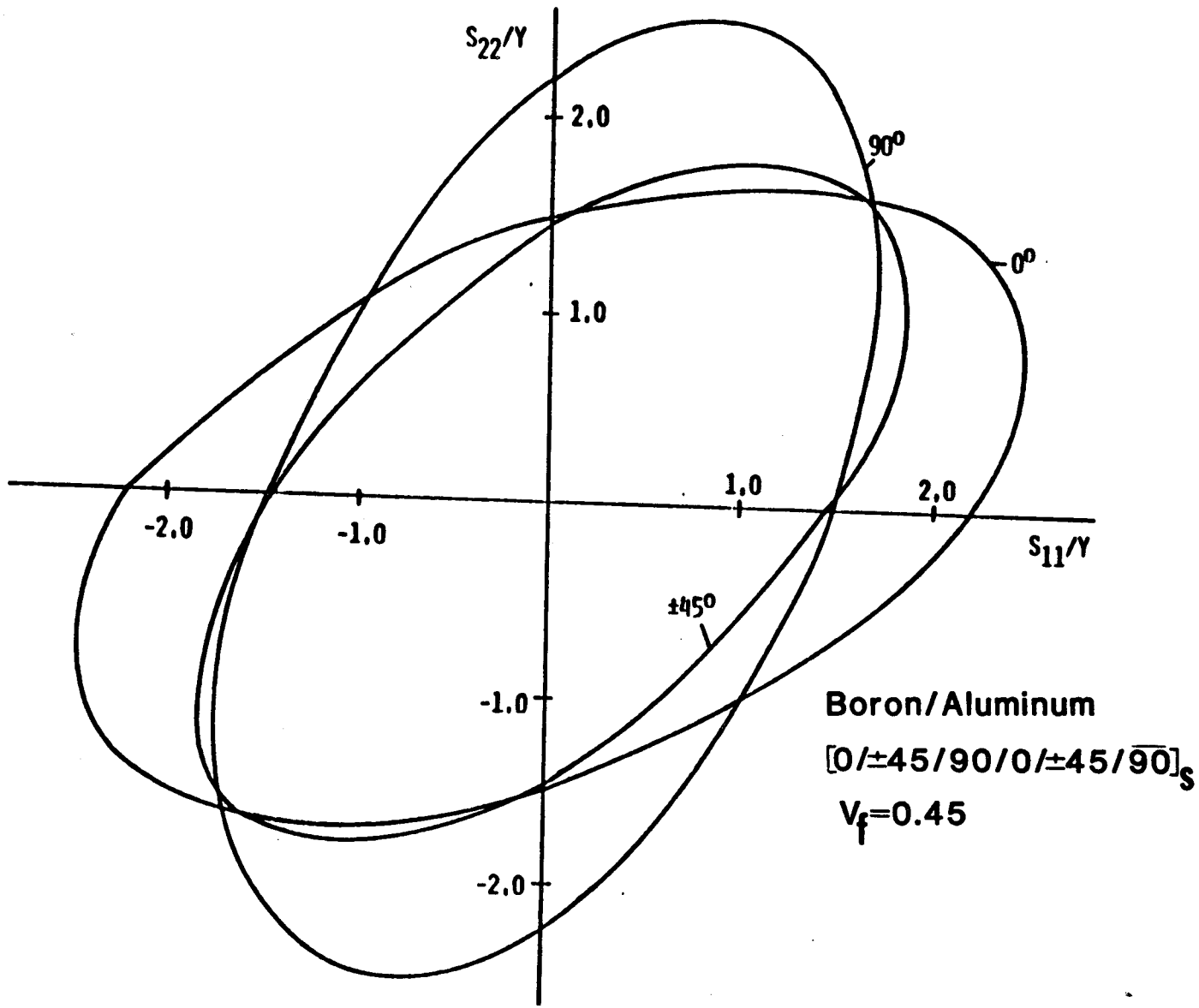

Figure 3. Yield surfaces of a B/Al laminated plate loaded by in-plane biaxial normal stresses. The S_{11} direction coincides with 0° fiber direction [18].

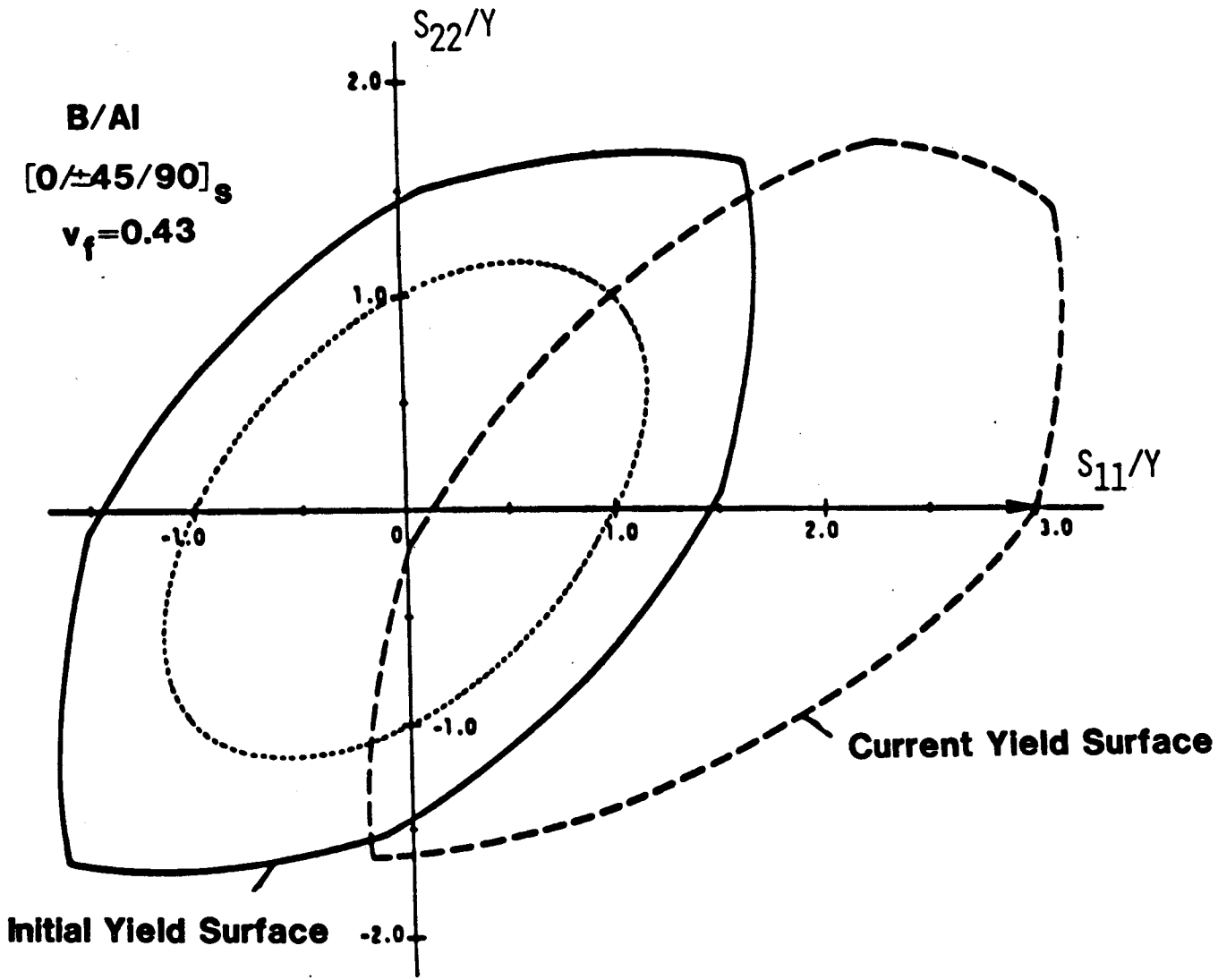

Figure 4. Initial and current yield surfaces of a B/Al laminated plate loaded by in-plane biaxial normal stresses. The S_{11} direction coincides with 0° fiber direction [18].

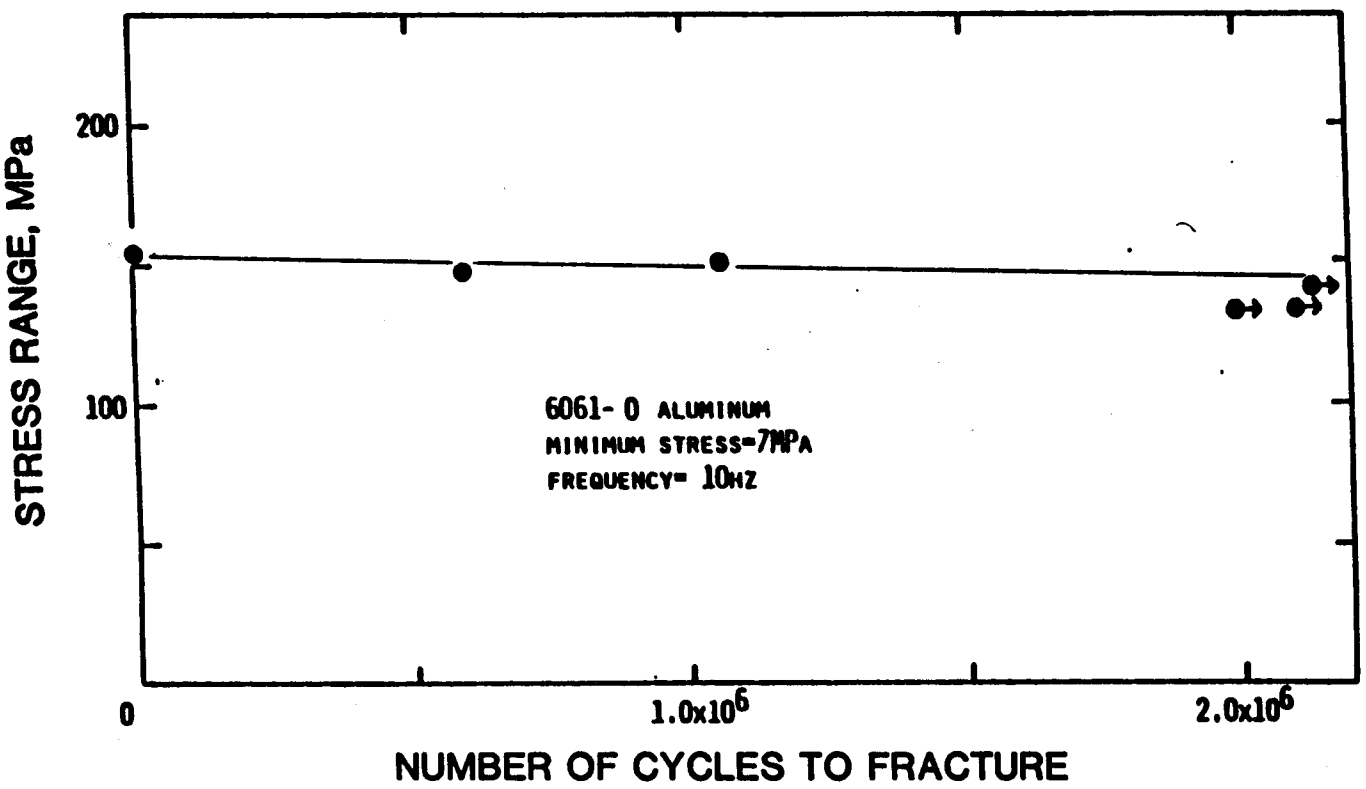

Figure 5. Fatigue test results for annealed aluminum matrix material [18].

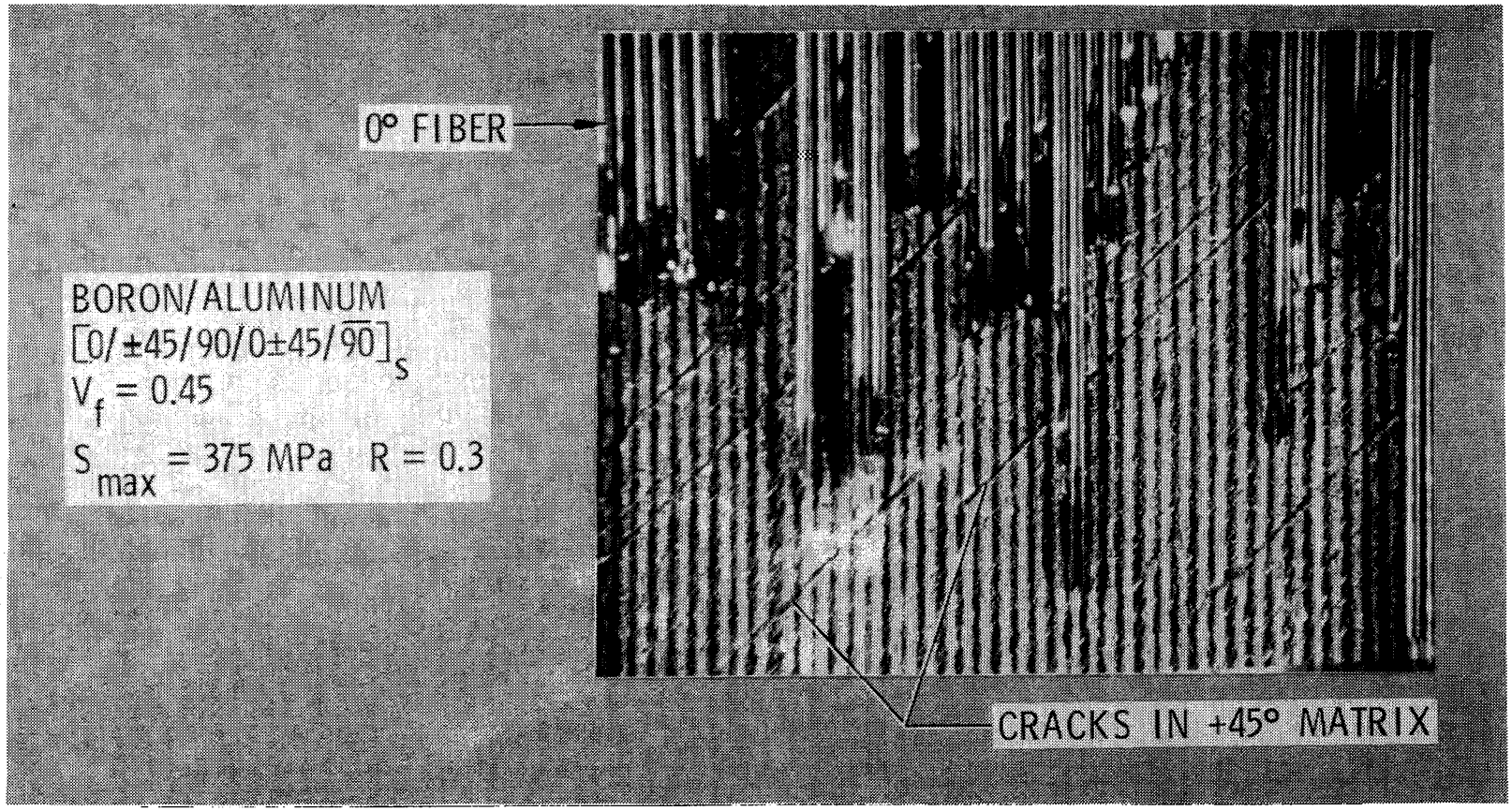

Figure 6. Cracks in the ±45° lamina matrix material at the saturation damage state [20].

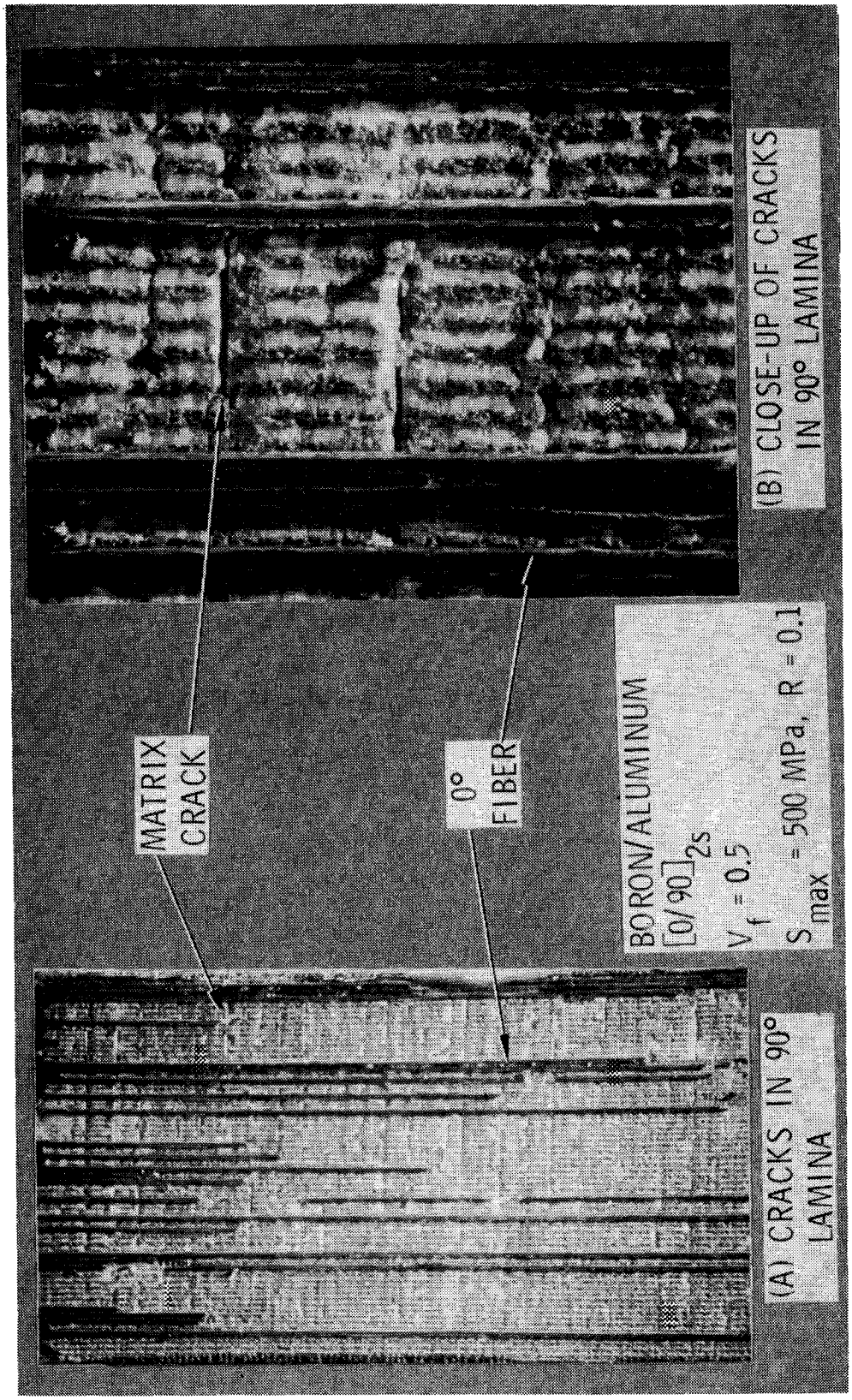

Figure 7. Cracks in 90-deg lamina matrix material [20].

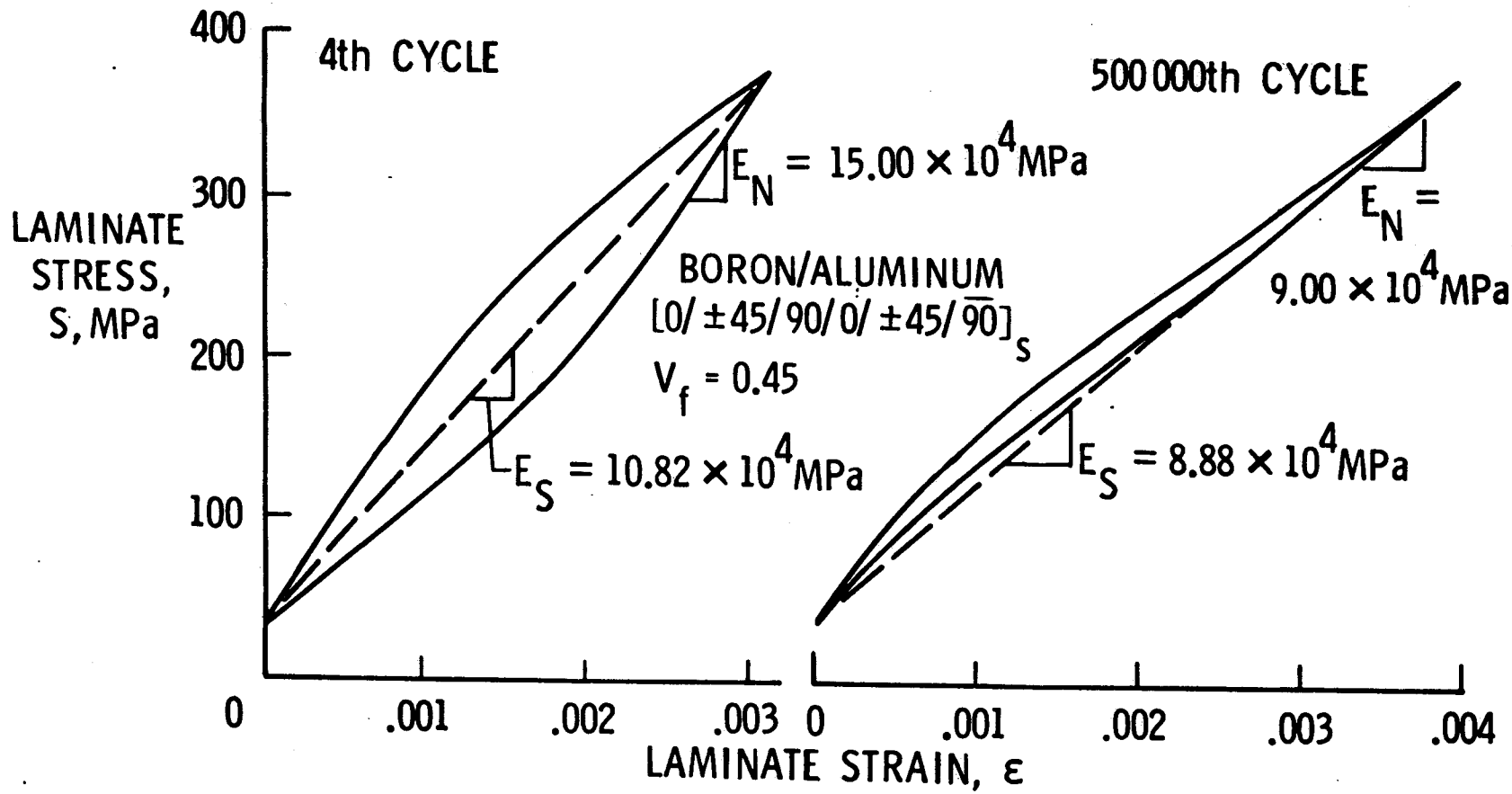

Figure 8. Observed moduli in the fourth cycle due to plasticity and observed moduli in the 500 000th cycle due to matrix cracking [21].

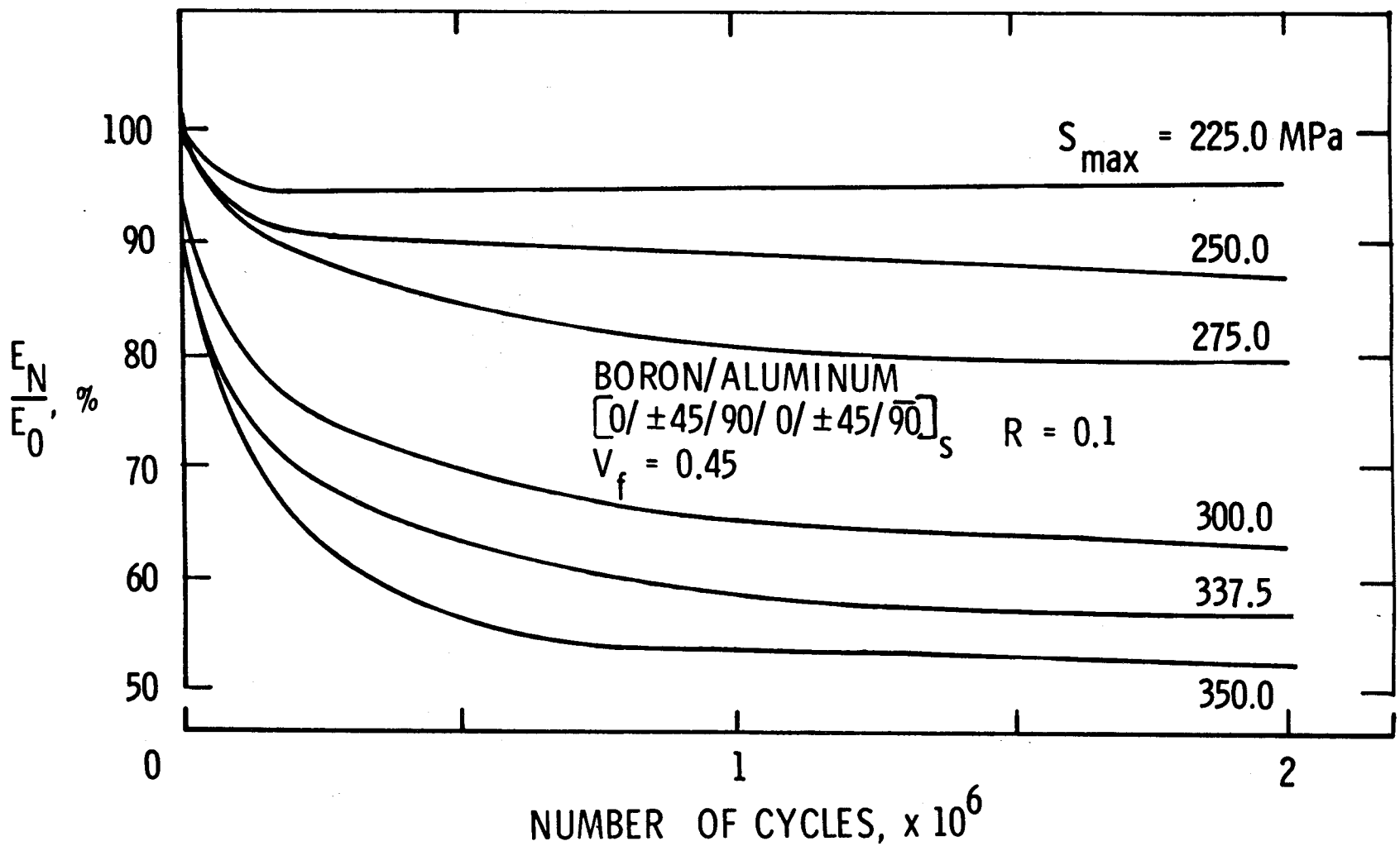

Figure 9. Change in elastic unloading modulus of $[0/\pm45/90/0/\pm45/\overline{90}]_S$ The specimen were tested at different values of S_{max} at R=0.1 [21].

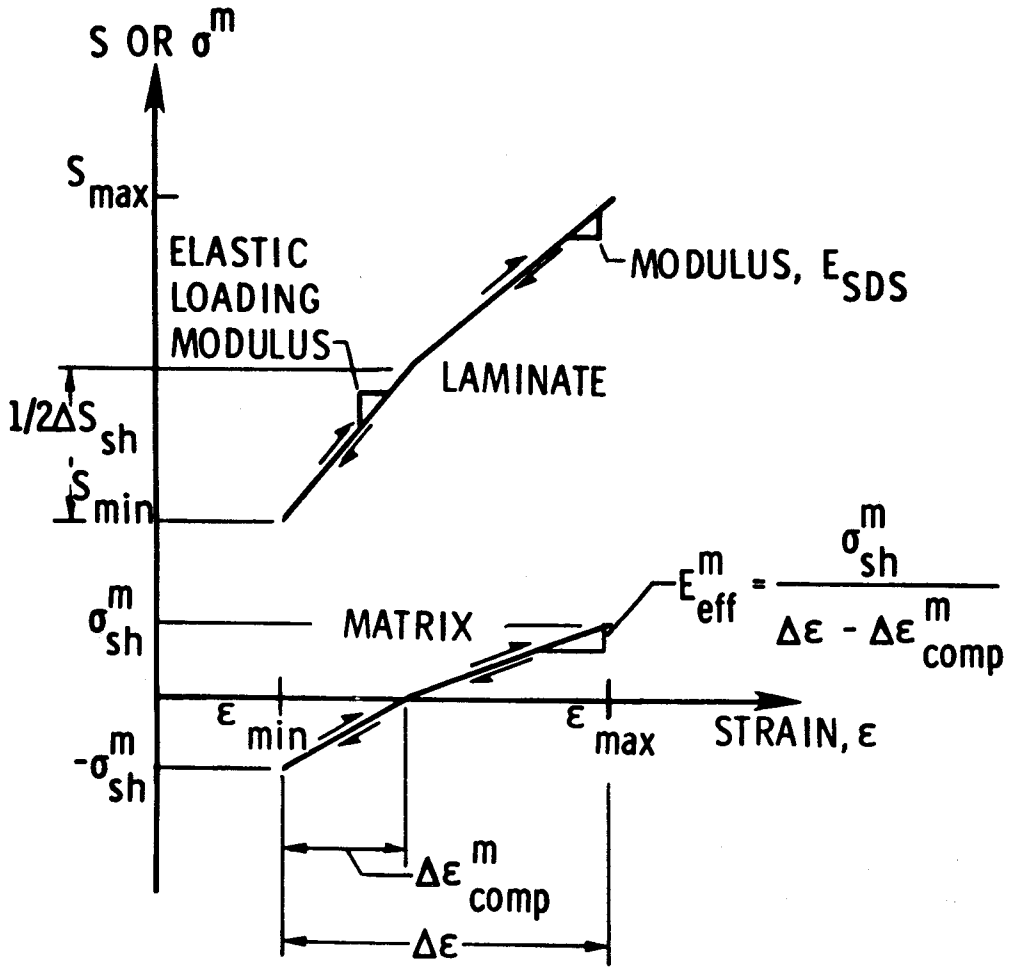

Figure 11. Composite laminate and matrix stress-strain response for a saturation damage state [21].

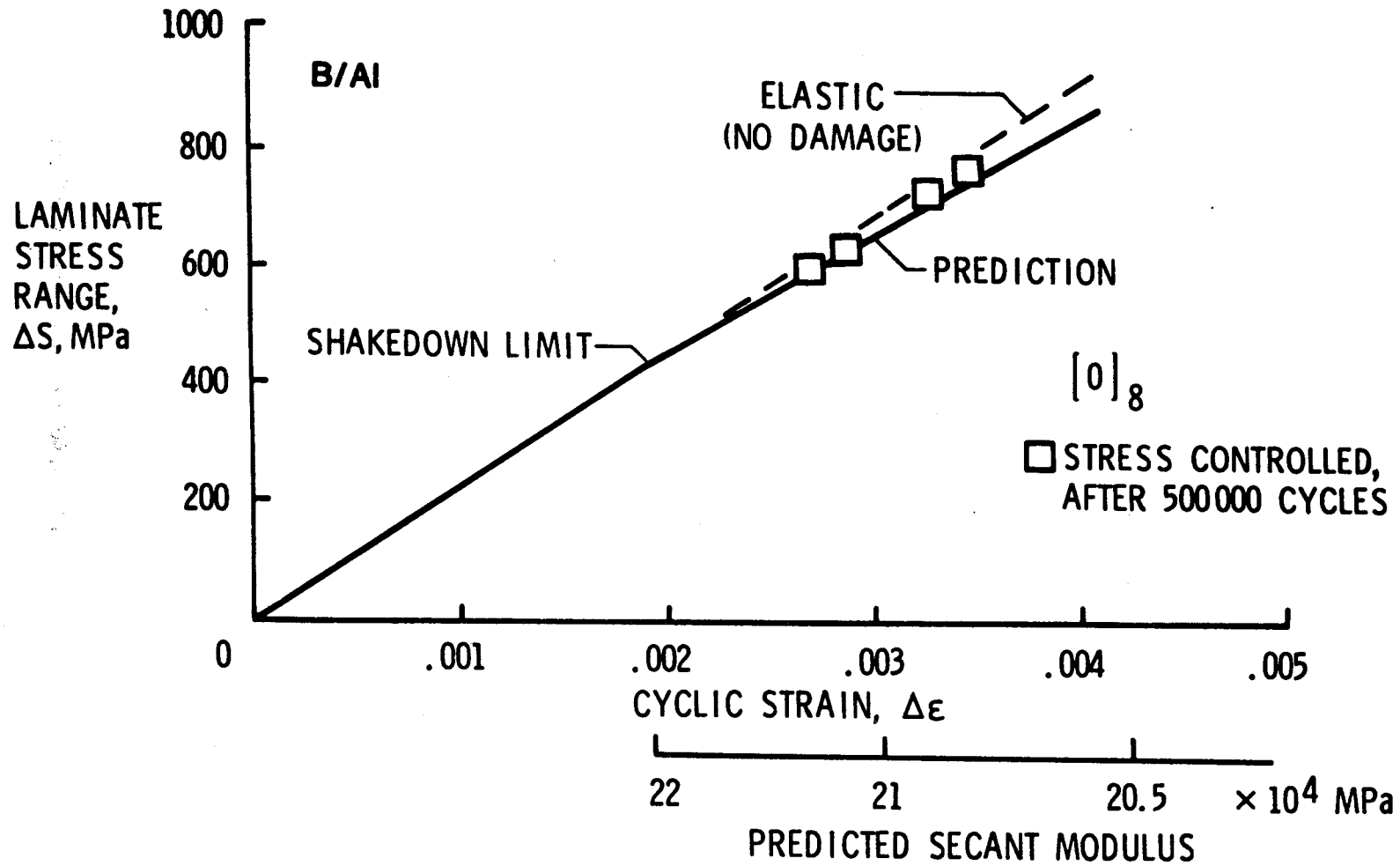

Figure 12. Correlation of experimental and model predictions for $[0]_8$ laminate after 500 000 fatigue cycles [21].

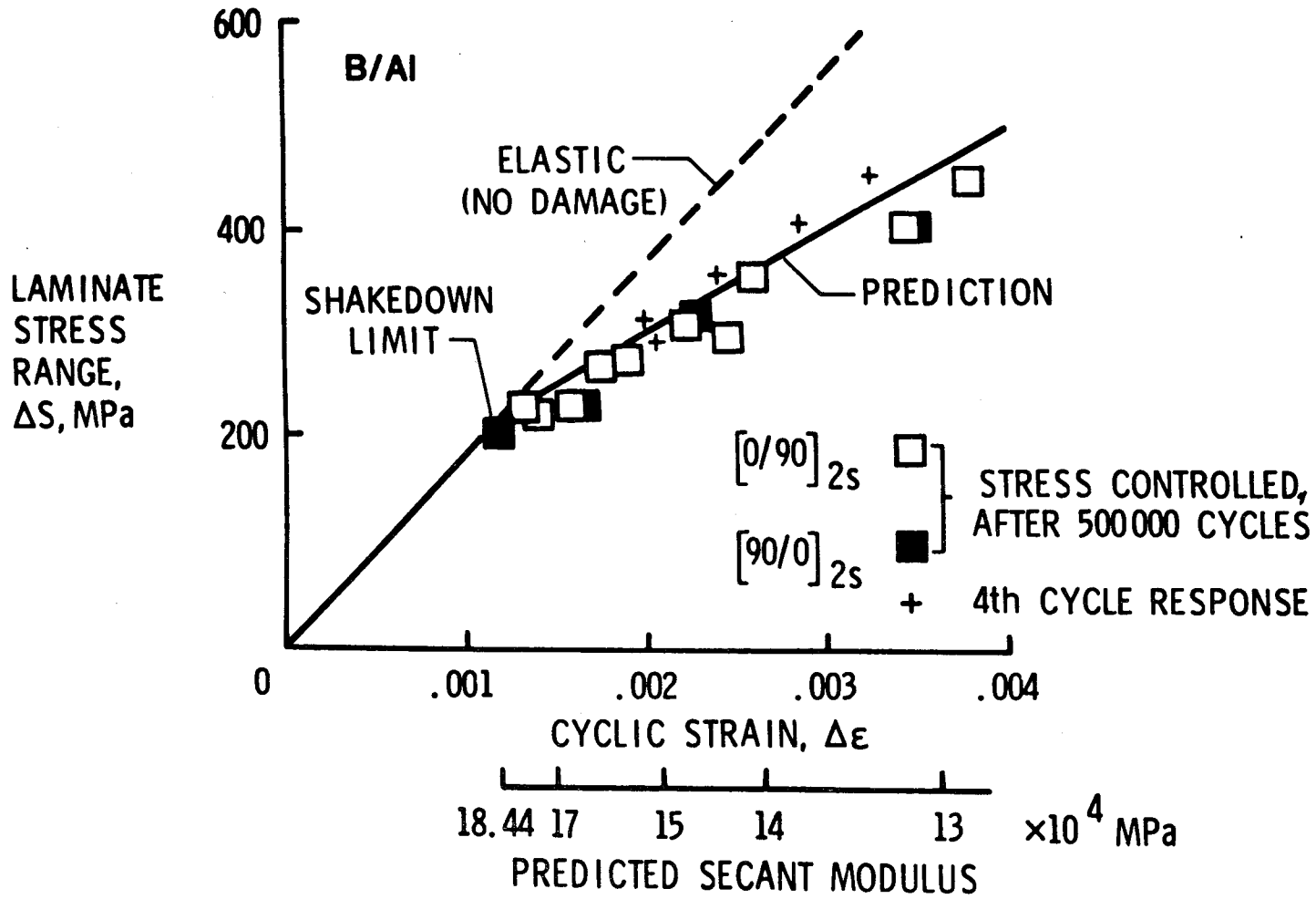

Figure 13. Correlation of experimental and model predictions for $[0/90]_{2S}$ and $[90/0]_{2S}$ laminates after 500 000 fatigue cycles. The cyclic response for the fourth cycle is shown for some specimens [21].

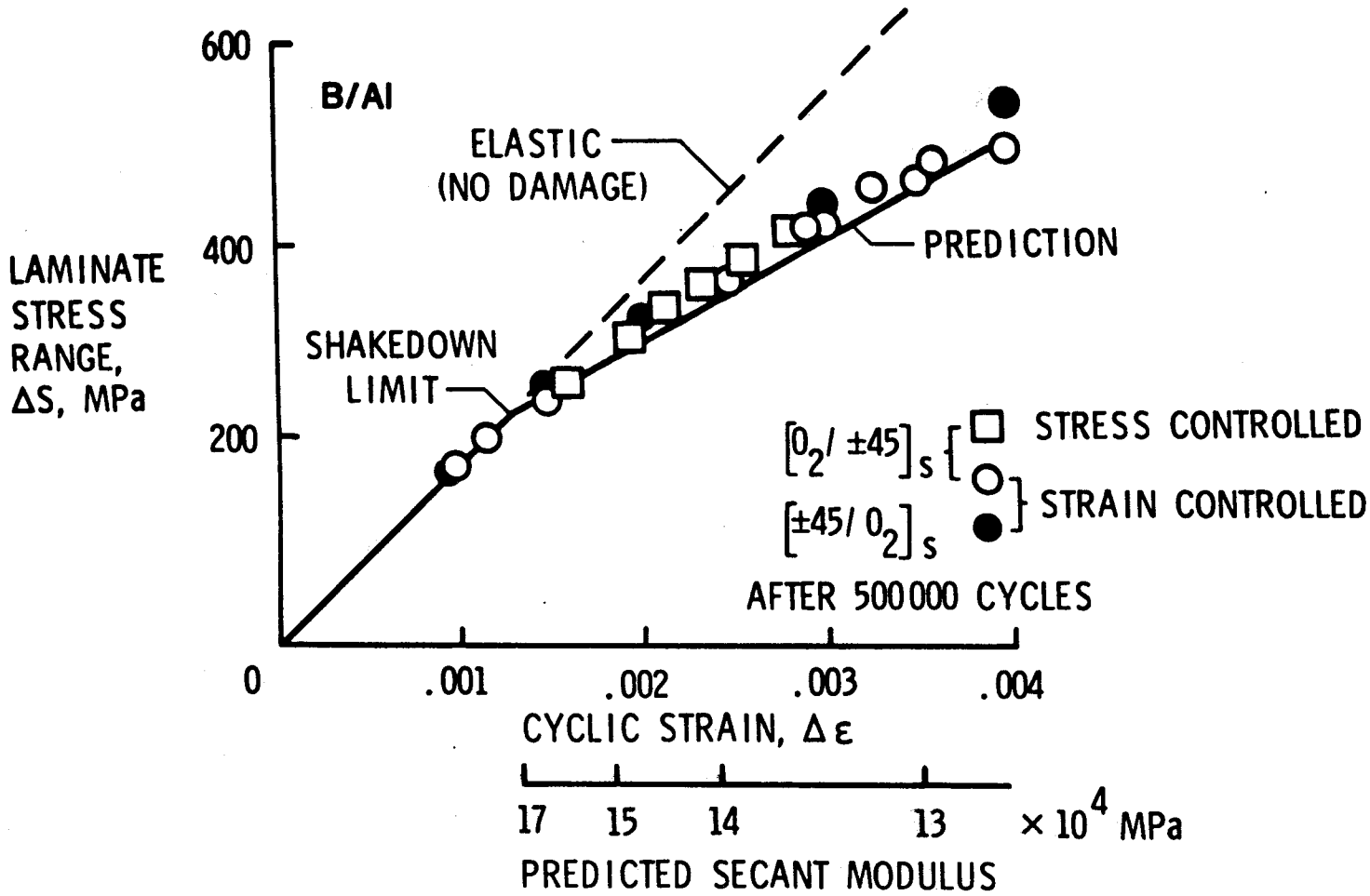

Figure 14. Correlation between experimental and model predictions for $[0_2/\pm45]_S$ and $[\pm45/0_2]_S$ laminates after 500 000 fatigue cycles [21].

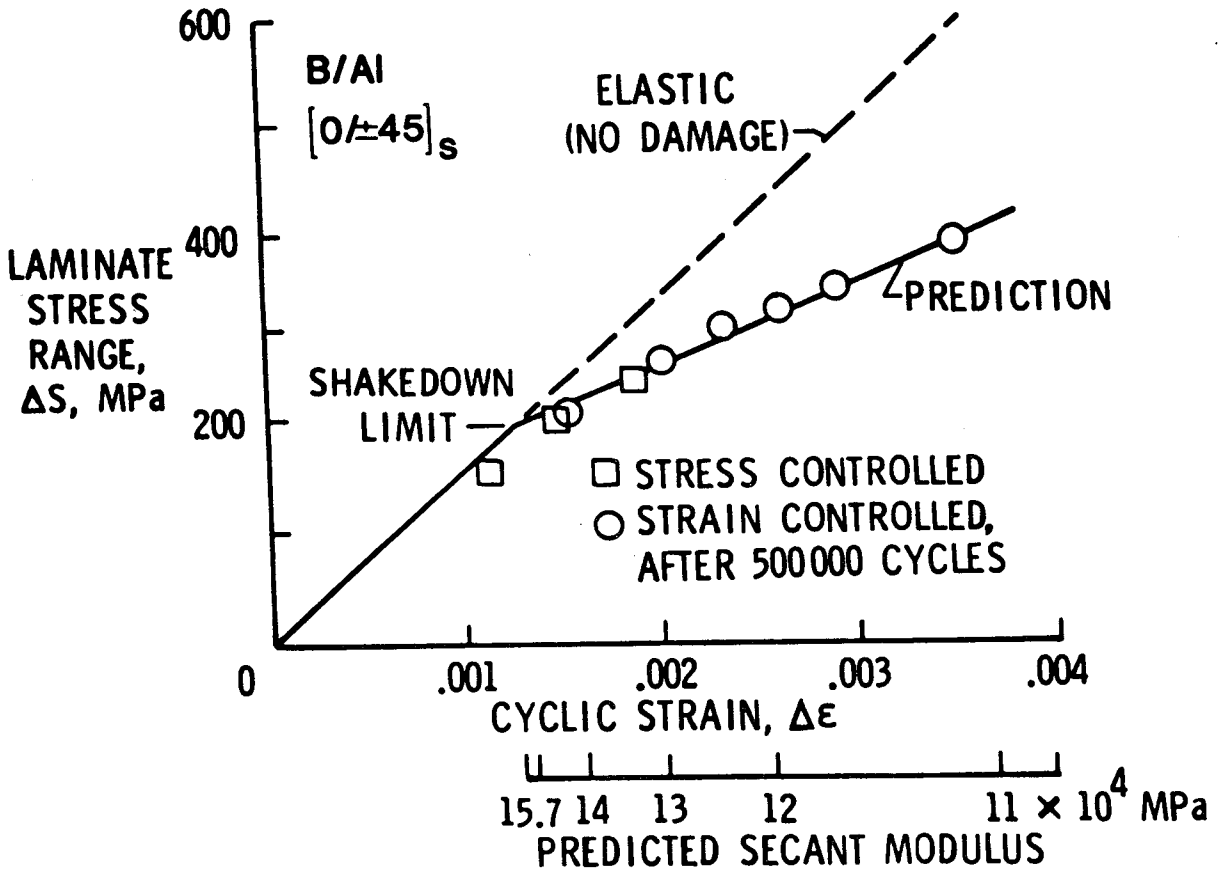

Figure 15. Correlation between experimental and model predictions for a $[0/\pm45]_S$ laminate after 500 000 fatigue cycles [21].

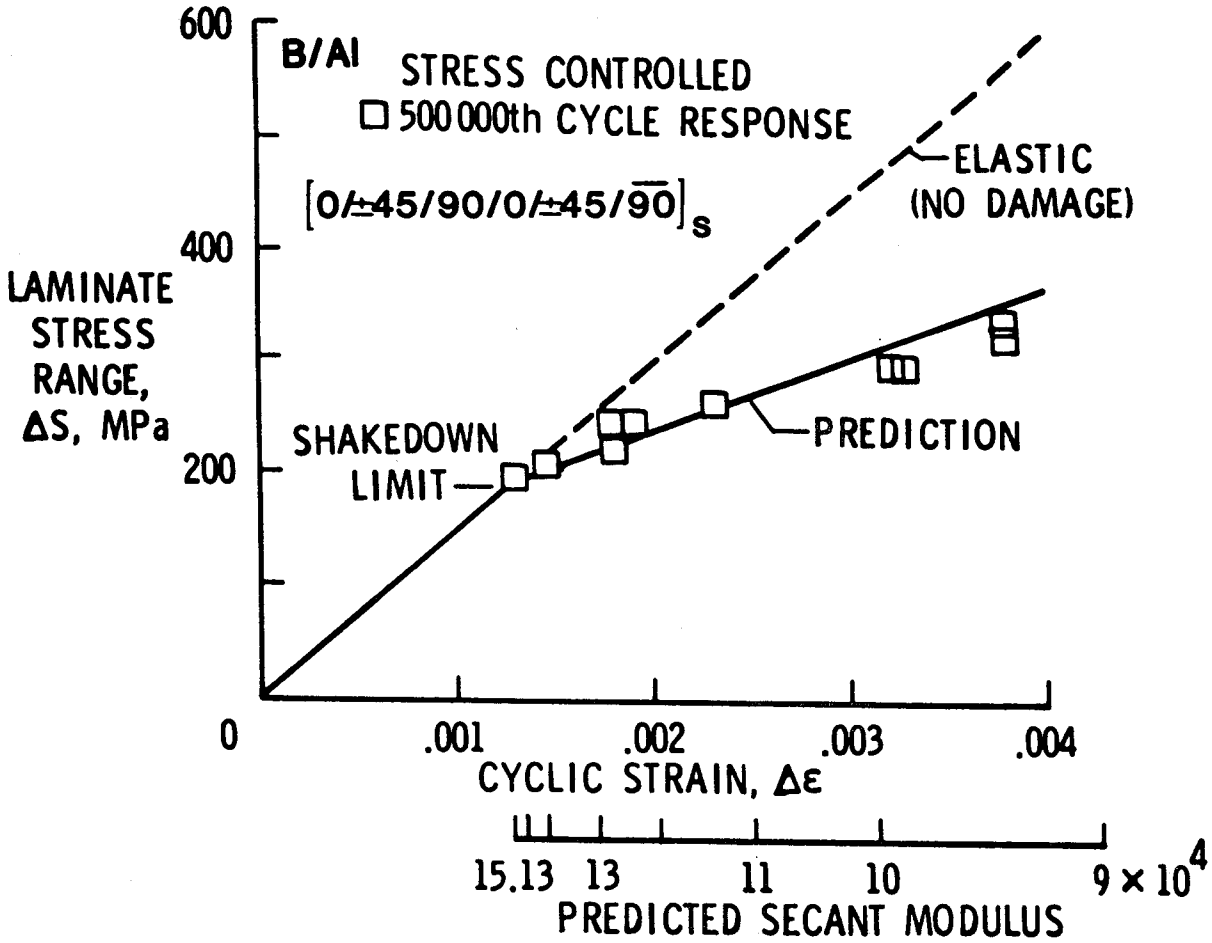

Figure 16. Correlation between experimental and model predictions for a $[0/\pm45/90/0/\pm45/\overline{90}]_S$ laminate after 500 000 fatigue cycles [21].

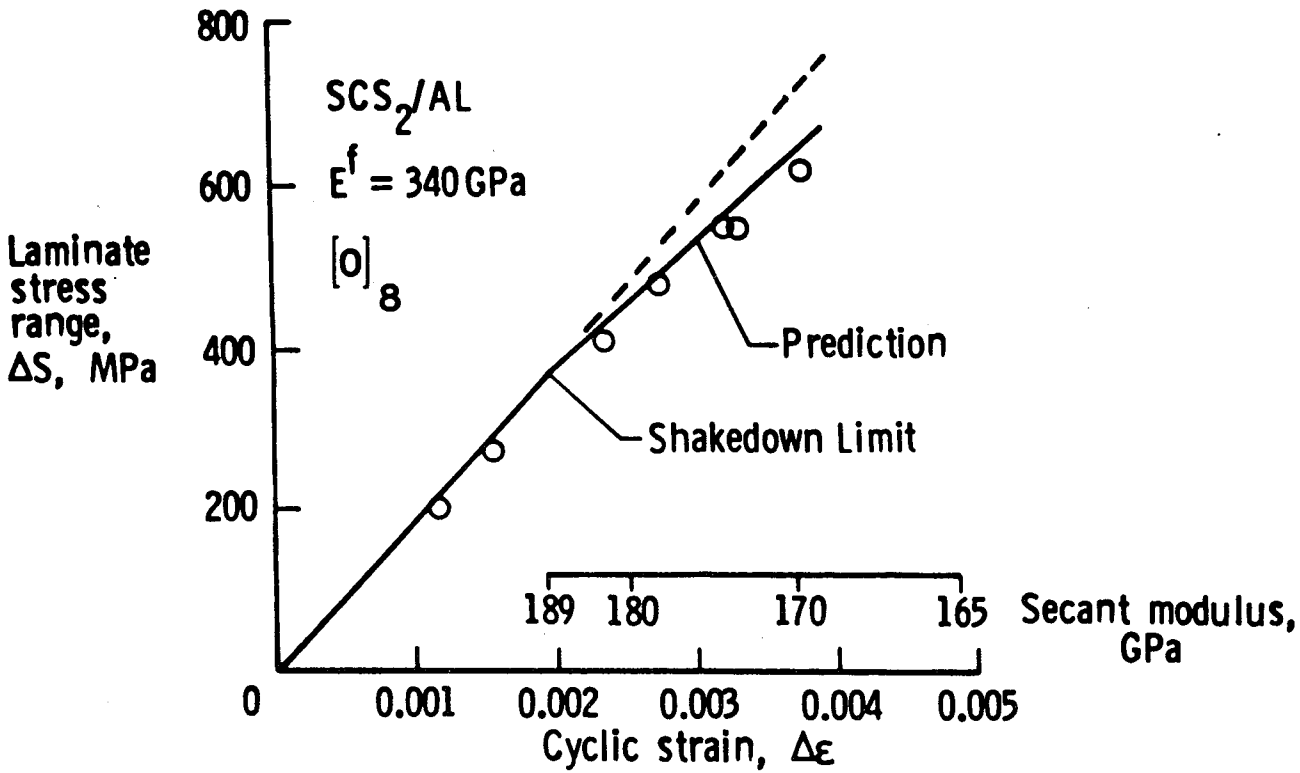

Figure 17. Correlation of experimental and model prediction for $[0]_8$ laminates after 500 000 Hz fatigue [26].

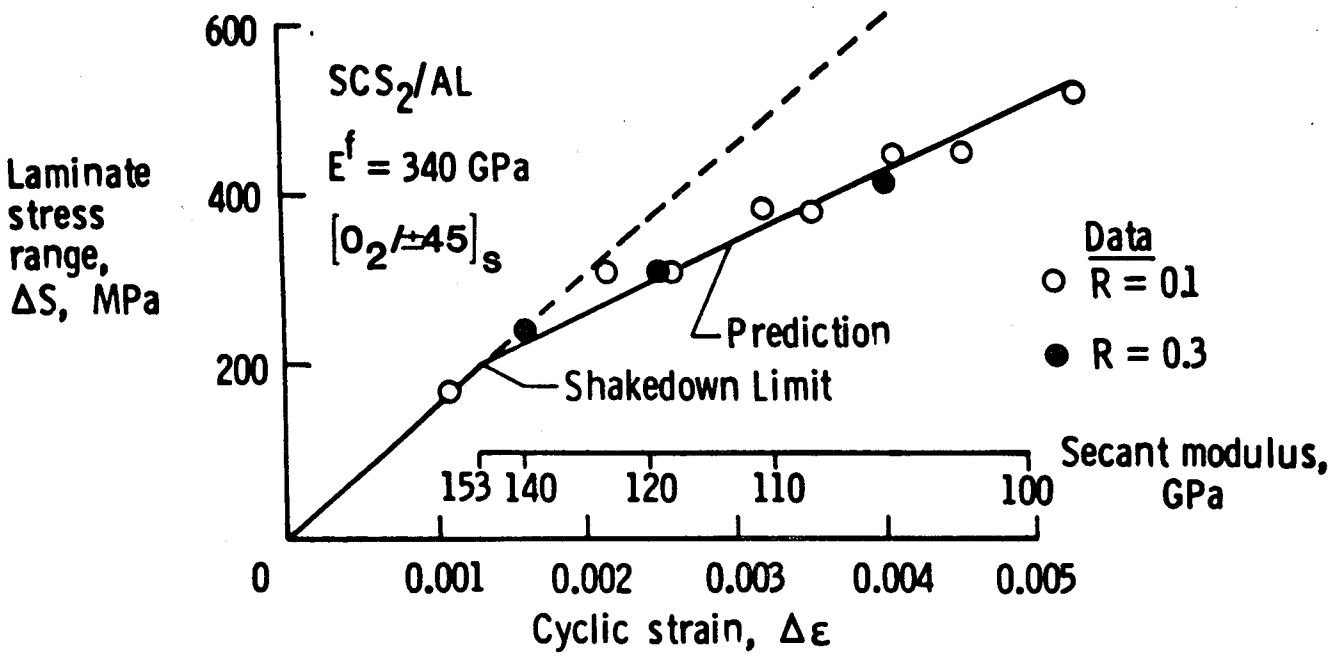

Figure 18. Correlation of experimental and model predictions for $[0_2/\pm45]$ laminates after 500 000 Hz fatigue [26].

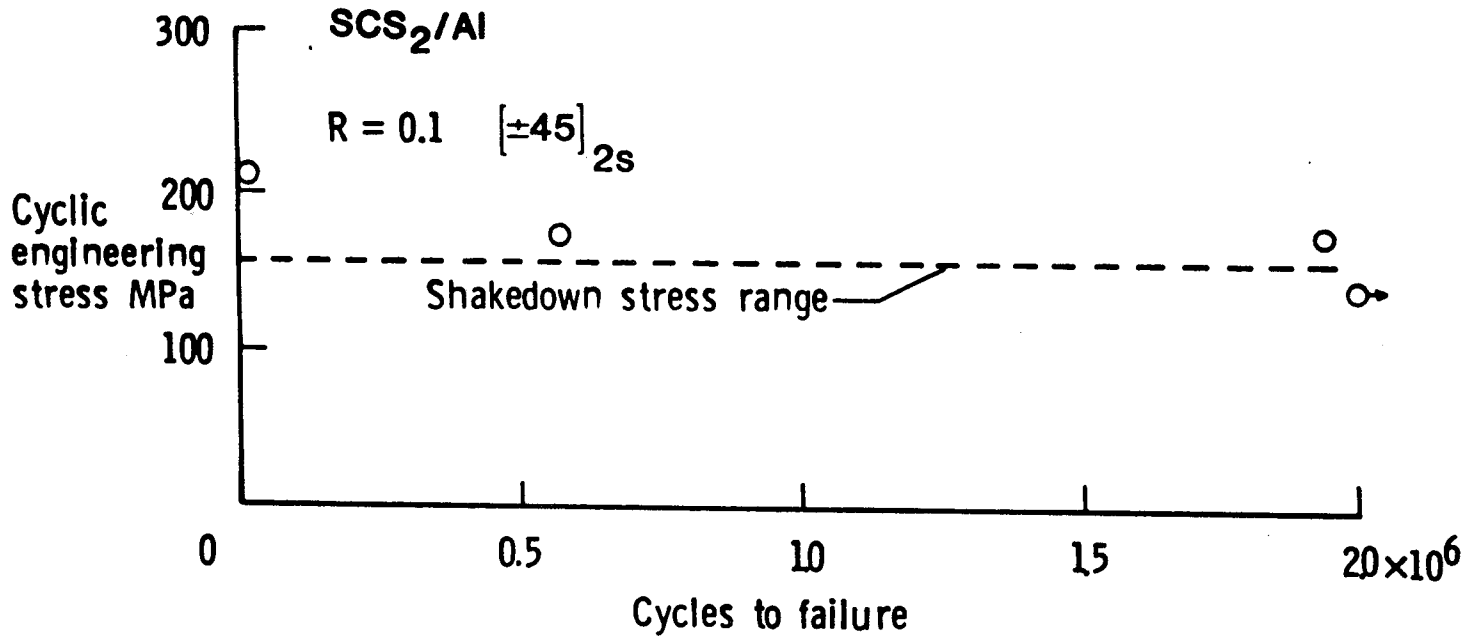

Figure 19. S-N curve for $[\pm 45]_{2S}$ laminates [26].

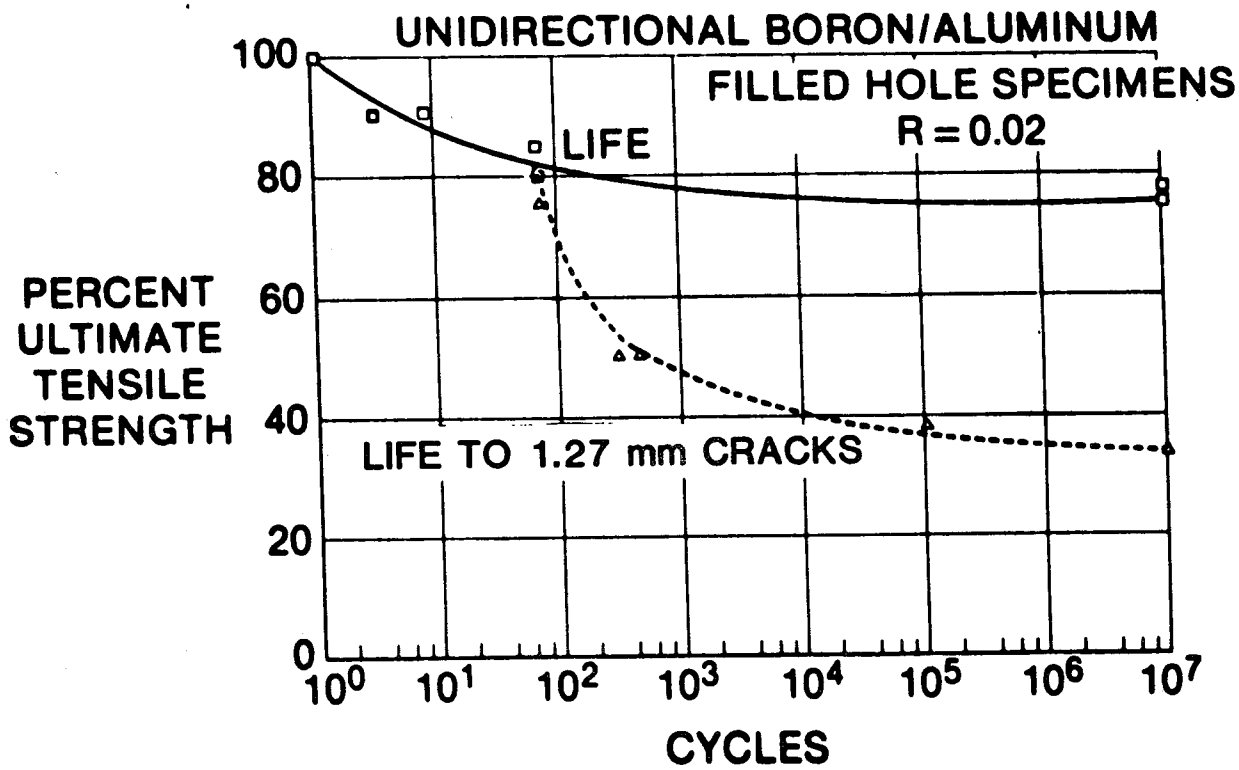

Figure 20. Matrix cracking and fiber failure curves in boron/aluminum [29]

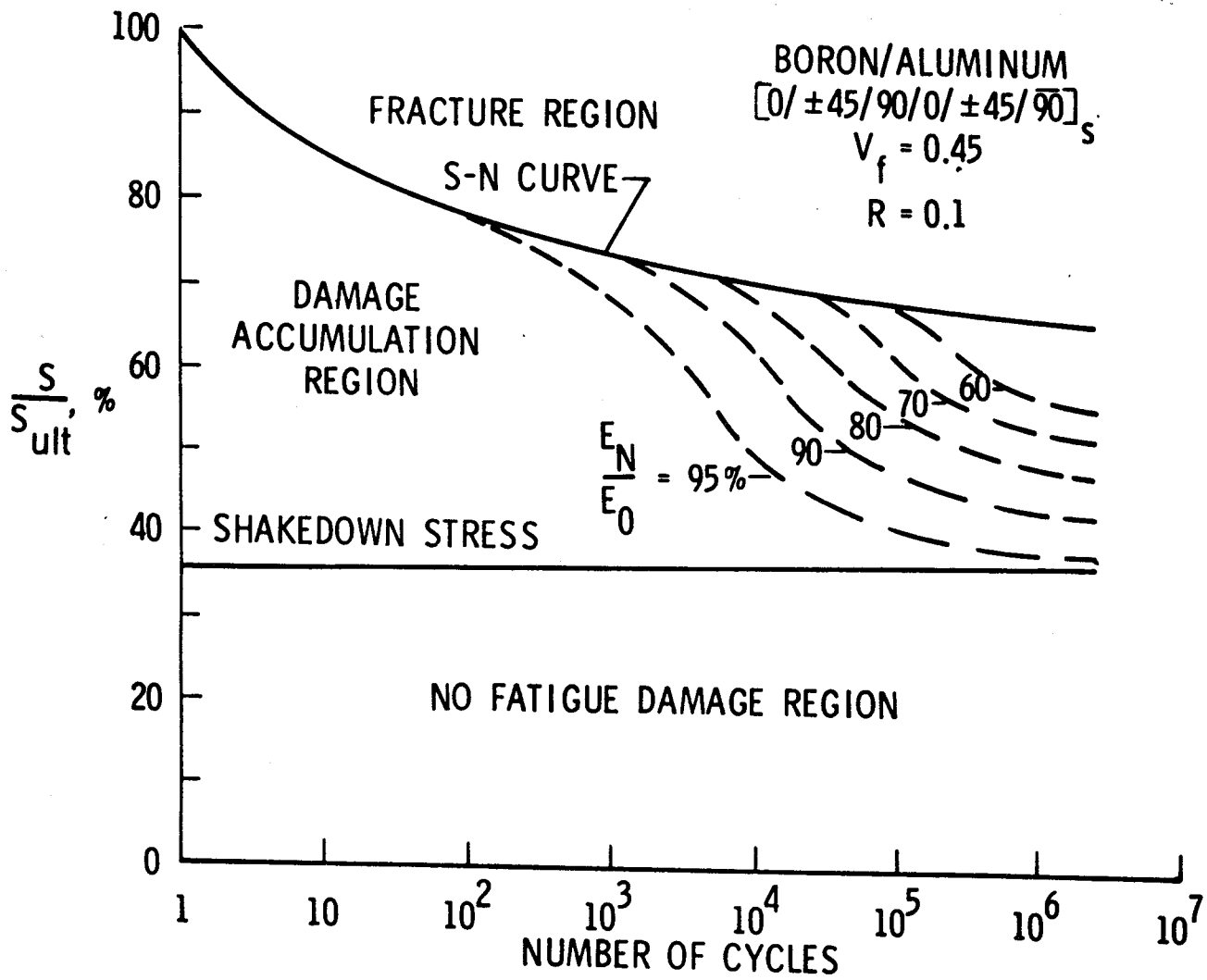

Figure 21. Three regions of response to fatigue loading.

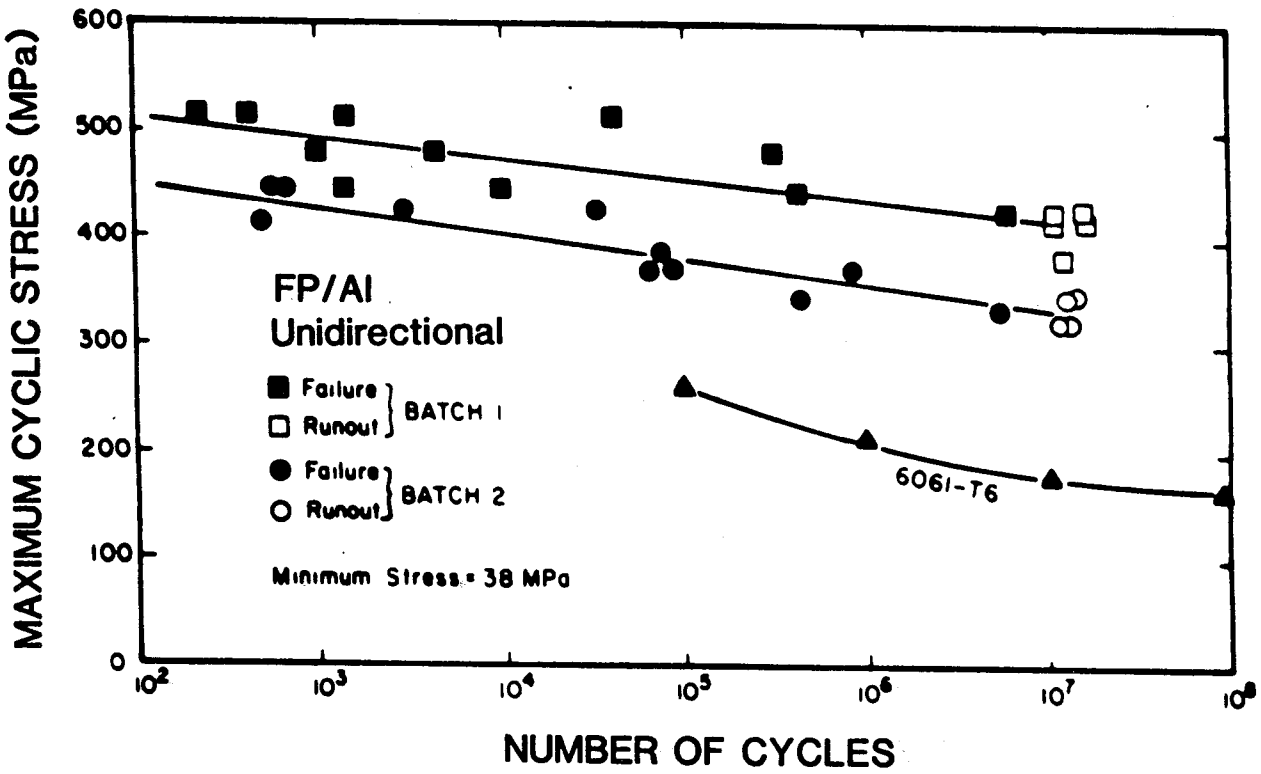

Figure 22. S-N curves for unidirectional FP/Al. 55% fiber volume fraction [32].

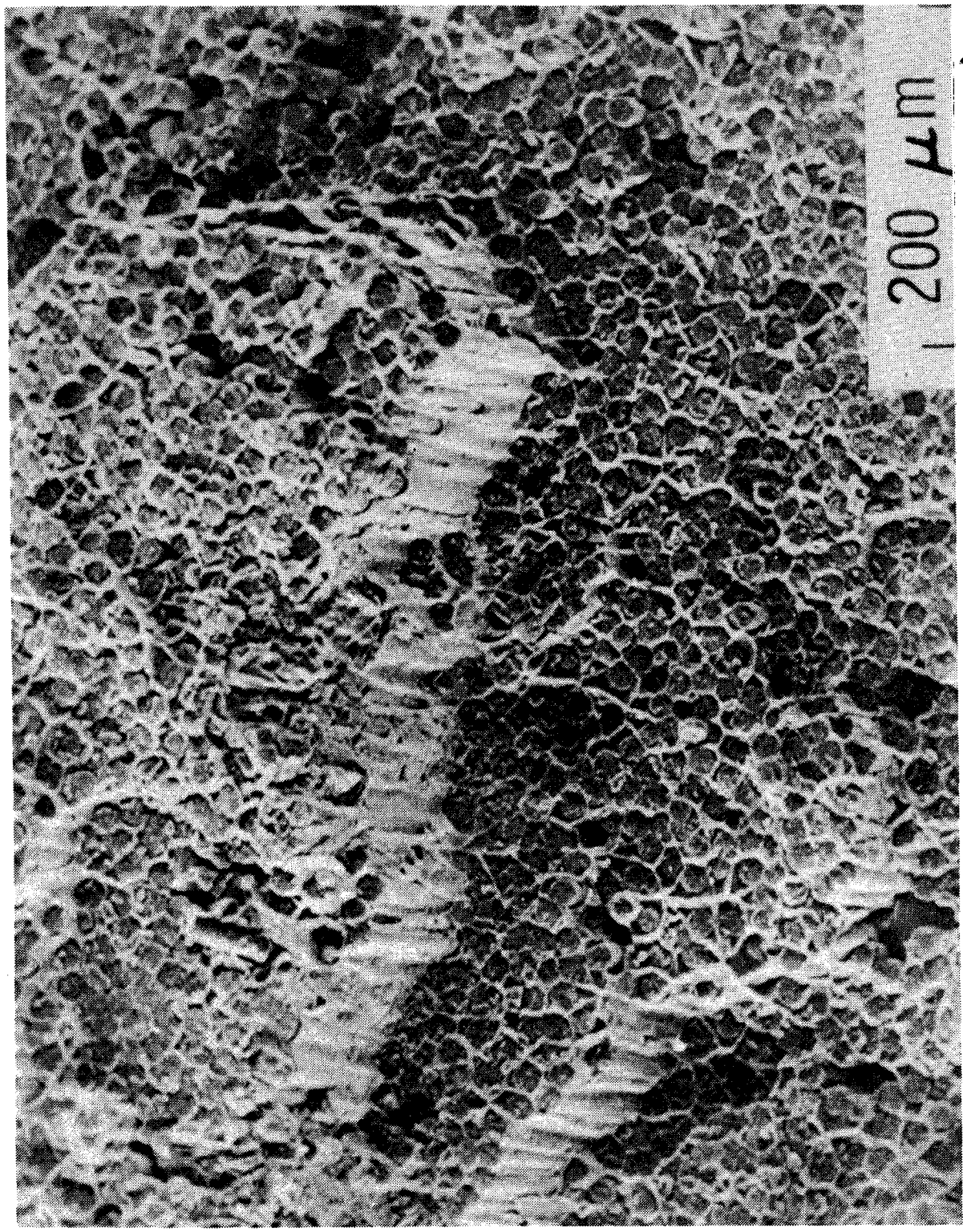

Figure 23. Typical SEM fracture surface topography for FP/Al [32].

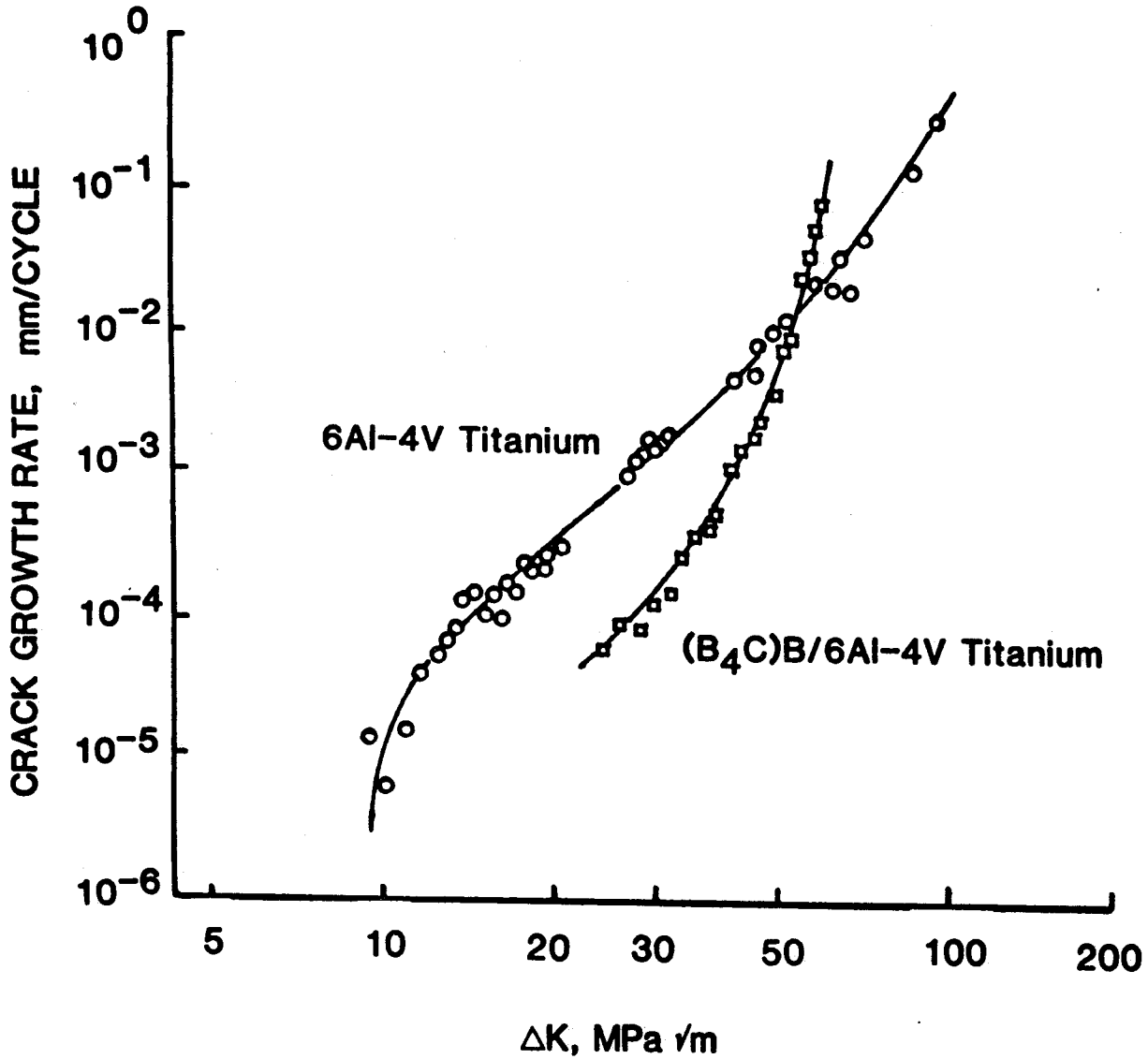

Figure 24. Crack growth in titanium with and without unidirectional fiber reinforcement [29].

Standard Bibliographic Page

1. Report No.	2. Government Accession No.	3. Recipient's Catalog No.
NASA TM-89116		

4. Title and Subtitle	5. Report Date
Fatigue Damage Accumulation in Various Metal Matrix Composites	March 1987
	6. Performing Organization Code: 505-63-01-05
7. Author(s): W. S. Johnson	8. Performing Organization Report No.
9. Performing Organization Name and Address: National Aeronautics and Space Administration, Langley Research Center, Hampton, VA 23665-5225	10. Work Unit No.
	11. Contract or Grant No.
12. Sponsoring Agency Name and Address: National Aeronautics and Space Administration, Washington, DC 20546	13. Type of Report and Period Covered: Technical Memorandum
	14. Sponsoring Agency Code

15. Supplementary Notes

This paper will appear as a book chapter entitled "Fatigue of Metal Matrix Composites," in Fatigue of Composite, K. L. Reifsnider, ed., Elsevier Applied Science, London, 1987,

16. Abstract

The purpose of this paper is to review some of the latest understanding of the fatigue behavior of continuous fiber reinforced metal matrix composites. The emphasis is on the development of an understanding of different fatigue damage mechanisms and why and how they occur. The fatigue failure modes in continuous fiber reinforced metal matrix composites are controlled by the three constituents of the system: fiber, matrix, and fiber/matrix interface. The relative strains to fatigue failure of the fiber and matrix will determine the failure mode. Several examples of matrix, fiber, and self-similar damage growth dominated fatigue damage are given for several metal matrix composite systems. Composite analysis, failure modes, and damage modeling are discussed. Boron/aluminum, silicon-carbide/aluminum, FP/aluminum, and borsic/titanium metal matrix composites are discussed.

17. Key Words (Suggested by Authors(s))	18. Distribution Statement
Metal matrix compostes Fatigue Boron/aluminum Silicon-carbide/aluminum FP/aluminum Borsic/aluminum	Unclassified - Unlimited Subject Category - 24

19. Security Classif.(of this report)	20. Security Classif.(of this page)	21. No. of Pages	22. Price
Unclassified	Unclassified	67	A04

For sale by the National Technical Information Service, Springfield, Virginia 22161